



Physical model inversion of the green spectral region to track assimilation rate in almond trees with an airborne nano-hyperspectral imager

L. Suarez^{a,*}, V. González-Dugo^b, C. Camino^c, A. Hornero^{b,d}, P.J. Zarco-Tejada^{a,b}

^a School of Agriculture and Food, Faculty of Veterinary and Agricultural Sciences (FVAS), Department of Infrastructure Engineering, Melbourne School of Engineering (MSE), University of Melbourne, Melbourne, Victoria, Australia

^b Instituto de Agricultura Sostenible (IAS), Consejo Superior de Investigaciones Científicas (CSIC), Avenida Menéndez Pidal s/n, 14004 Córdoba, Spain

^c European Commission (EC), Joint Research Centre (JRC), Ispra (VA), Italy

^d Department of Geography, Swansea University, SA2 8PP Swansea, United Kingdom

ARTICLE INFO

Keywords:

Assimilation
Photosynthesis
Hyperspectral
Radiative transfer model
RTM
SCOPE
 $V_{c_{max}}$
Green spectral region
Fluorescence
SIF
PRI
Nano-Hyperspec

ABSTRACT

Significant advances toward the remote sensing of photosynthetic activity have been achieved in the last decades, including sensor design and radiative transfer model (RTM) development. Nevertheless, finding methods to accurately quantify carbon assimilation across species and spatial scales remains a challenge. Most methods are either empirical and not transferable across scales or can only be applied if highly complex input data are available. Under stress, the photosynthetic rate is limited by the maximum carboxylation rate ($V_{c_{max}}$), which is determined by the leaf biochemistry and the environmental conditions. $V_{c_{max}}$ has been connected to plant photoprotective mechanisms, photosynthetic activity and chlorophyll fluorescence emission. Recent RTM developments such as the Soil-Canopy Observation of Photosynthesis and Energy fluxes (SCOPE) model allow the simulation of the sun-induced chlorophyll fluorescence (SIF) and $V_{c_{max}}$ effects on the canopy spectrum. This development provides an approach to retrieve $V_{c_{max}}$ through RTM model inversion and track assimilation rate. In this study we explore SIF, narrow-band indices and RTM inversion to track changes in photosynthetic efficiency as a function of vegetation stress. We use hyperspectral imagery acquired over an almond orchard under different management strategies which affected the assimilation rates measured in the field. $V_{c_{max}}$ used as an indicator of assimilation was retrieved through SCOPE model inversion from pure-tree crown hyperspectral data. The relationships between field-measured assimilation rates and $V_{c_{max}}$ retrieved from model inversion were higher ($r^2 = 0.7-0.8$) than when SIF was used alone ($r^2 = 0.5-0.6$) or when traditional vegetation indices were used ($r^2 = 0.3-0.5$). The method was proved successful when applied to two independent datasets acquired at two different dates throughout the season, ensuring its robustness and transferability. When applied to both dates simultaneously, the results showed a unique significant trend between the assimilation measured in the field and $V_{c_{max}}$ derived using SCOPE ($r^2 = 0.56$, $p < 0.001$). This work demonstrates that tracking assimilation in almond trees is feasible using hyperspectral imagery linked to radiative transfer-photosynthesis models.

1. Introduction

The accurate monitoring of plant photosynthetic activity at large scales is required to control the effects of potential threats affecting adequate growth and resulting yield (Kimball 1983; Lobell et al. 2009; Long et al. 2015). Plants under water and nutrient stress regulate their photosynthetic rate reducing the production of assimilates (Schurr et al. 2006). Non-photochemical dissipation mechanisms protect the photosynthetic apparatus from excessive absorbed energy. These photoprotective mechanisms are very dynamic with illumination intensity

and react within seconds or minutes (Demmig et al. 1987). The timely assessment of crop stress is therefore challenging as when symptoms are visually detectable, productivity and yield might be compromised (Hsiao et al. 1976; Hsiao and Bradford 1983). In the particular case of orchards, in addition to frequent monitoring, the within-field heterogeneity resulting from changes in elevation, soil and irrigation system efficiency requires methods that properly assess the spatial variability of photosynthetic activity at the individual object level, e.g. at the tree scale. In the last decades, there has been an important advance toward developing remote sensing methods to detect pre-visual stress, that is

* Corresponding author.

E-mail address: l.suarez@unimelb.edu.au (L. Suarez).

before visual symptoms appear, and extend the assessment to describe within field variations (Chaerle, L., 2007; Suarez et al., 2009; Tremblay et al. 2011; Zarco-Tejada et al. 2012; Ihuoma and Madramootoo 2017; Hernandez-Clemente et al., 2019).

Changes in both the green spectral region and in the emission of chlorophyll fluorescence from photosystem I (PS-I) and photosystem II (PS-II) have been connected to plant photosynthetic dynamic processes under stress (Lichtenthaler et al., 1998; Papageorgiou 1975; Gamon et al. 1992; Krause and Weis 1991; Mohammed et al. 2019). The effect in the green region has been attributed to photoprotective mechanisms that dissipate part of the absorbed radiation under limited photosynthetic capacity, mainly through changes in xanthophyll pigment composition (Demmig-Adams 1990). When incoming radiation exceeds the capacity of the photosynthetic reaction centres, the xanthophyll pigment violaxanthin (V) de-epoxidise to antheraxanthin (A) and later to zeaxanthin (Z) to avoid oversaturation. This process has an effect on the spectral signal around 531 nm and has been used to track photosynthetic efficiency remotely (Gamon et al. 1992, Filella et al. 1996, Styliński et al. 2000; Evain et al. 2004).

As a proxy of photosynthesis activity, the chlorophyll fluorescence signal can be quantified as the ratio between the maximum variable fluorescence emission to the maximum total fluorescence (Krause and Weis 1991; Mohammed et al. 1995). The application of this method to image data is not practical though, being the focus on quantifying steady-state fluorescence signals, i.e. SIF, for the remote assessment. Among other methods, SIF can be quantified applying the Fraunhofer Line Depth (FLD) principle using the atmospheric O₂ absorption bands (Plascyk and Gabriel 1975). Despite the high spectral resolution required to quantify fluorescence at the O₂-A and O₂-B absorption bands, modelling work by Damm et al. (2011) demonstrated that sensors with 5–6 nm full-width at half maximum (FWHM) spectral bands within the oxygen absorption window can be used to derive sun-induced fluorescence through this method. As an example, Zarco-Tejada et al. (2012, 2016, 2018) and Damm et al. (2014, 2015a) showed successful retrievals of sun-induced fluorescence (SIF) using airborne sensors of such spectral characteristics in the context of stress detection, e.g. focusing on the relative spatial variability of SIF as an indicator of stress.

Although SIF has been demonstrated to be directly linked to photosynthetic activity (Mohammed et al. 2019; Meroni et al. 2009; Rascher et al. 2009; Zarco-Tejada et al. 2009), the amount of fluorescence emitted and its quantification based on the in-filling method described above is affected by the irradiance levels at the time of data acquisition, therefore highly variable in the temporal scale. Indices derived from the green region present similar issues when used with time series of image data (Gamon et al. 1997; Damm et al. 2015b). Attempts to normalise these indices calculated from reflectance and FLD methods with ancillary measurements have been frequent in the last years (Suarez et al., 2010; Zarco-Tejada et al. 2013b). Apart from the difficulties to properly normalise these spectral indices, the link between these indicators and photosynthetic efficiency needs to be established to provide a meaningful interpretation (Nichol et al. 2002; Running et al. 1999). This link is typically highly empirical, site and species specific (Courault et al. 2005) and affected by structural and pigment levels across species.

The estimation of photosynthetic parameters (i.e. $V_{c_{max}}$) is an alternative approach that does not rely on further empirical links. The limitation in the enzyme kinetic processes driving photosynthesis is defined by two parameters, the maximum electron transport rate (J_{max}) and the maximum carboxylation rate ($V_{c_{max}}$) by the Ribulose-1,5-bisphosphate carboxylase/oxygenase (RuBisCO) enzyme under saturated light conditions. Both $V_{c_{max}}$ and J_{max} change in response to environmental conditions and the CO₂ fixation rate is determined by the most limiting of them (Farquhar et al. 1980). $V_{c_{max}}$ has been proposed as a useful parameter linked to photosynthetic rate, given its responsiveness to biotic and abiotic stressors, such as insect or pathogen damage (Dungan et al. 2007) and drought (Xu and Baldocchi 2003). In the field, $V_{c_{max}}$ is obtained from leaf measurements made with a gas exchange

instrument using net assimilation of CO₂–intercellular CO₂ concentration (A–Ci) curves (Farquhar et al. 1980). However, measuring $V_{c_{max}}$ on the ground is time-consuming and logistically impossible for timely large-area assessments of the natural heterogeneity present in agricultural fields.

Empirical models derived by Serbin et al. (2012, 2015) showed there is a strong spectral response to $V_{c_{max}}$ changes in the blue-green and the Red-Edge spectral regions but reached the conclusion that there is not unique link between spectral signal and $V_{c_{max}}$ and the large-area assessment of $V_{c_{max}}$ based on spectral data needed to account for species type and environmental factors at the time of image acquisition. Recent advances in physical models have linked the radiative transfer theory with plant physiological modules where photosynthetic performance can be simulated as a function of stress and environmental conditions (Van der Tol et al. 2009). This is the case of the Soil Canopy Observation, Photochemistry and Energy fluxes model (SCOPE, Van der Tol et al. 2009). The SCOPE model allows the simulation of the effect of varying $V_{c_{max}}$ on the canopy spectra including the emission as fluorescence. According to model simulations presented in this study, these effects are spectrally located in the green (505–560 nm) and in the red and far-red chlorophyll fluorescence emission (650–850 nm) regions. By establishing the physical link between the spectral signal and $V_{c_{max}}$, changes in photosynthetic activity can be tracked without relying on site specific empirical relationships.

With the recent progress on the estimation of SIF at the global scale (Frankenberg et al. 2011; Guanter et al. 2014), especial interest has been put on models such as SCOPE for carbon accounting (Koffi et al. 2015). Some studies have demonstrated the big potential of SCOPE in combination with satellite-derived SIF to monitor carbon sequestration against international agreement targets (Zhang et al. 2014; Guan et al., 2016), although the spatial resolution of SIF derived from satellite imagery poses many challenges related to pixel heterogeneity and ancillary input data availability (Verma et al. 2017) which makes its interpretation complex. These challenges could be overcome by increasing the model capabilities to properly simulate the within-pixel heterogeneity. Increasing image spatial resolution to minimise the effect of mixed scene elements is another potential solution.

At the finer scale and in the context of precision agriculture, the assessment of $V_{c_{max}}$ through physical models might provide an advantage for the quantitative monitoring of canopy assimilation over time without relying on empirical methods that are not robust across scales and environmental conditions. As a photosynthetic trait, $V_{c_{max}}$ does not require any further link or empirical calculation to track assimilation over time. As an example, Camino et al. (2019) demonstrated the retrieval of $V_{c_{mo}}$ (e.g. $V_{c_{max}}$ of a top leaf standardized to a reference temperature at 25 °C) through SCOPE radiative transfer model inversion to track photosynthetic rate differences in wheat under nutrient and water stress.

The SCOPE model simulates the canopy as a 1D homogeneous flat turbid medium (Van der Tol et al. 2009; Verhoef 1984). This arrangement is ideal to simulate continuous crops like wheat but might be limited when attempting the same with discontinuous woody vegetation structures. Heterogeneous canopy scenes (i.e. tree orchards) present a complex arrangement of canopy, sunlit soil background and shadows (Verstraete et al. 1990; Law et al. 2001) adding complexity to the simulation of the multiple scattering effects between the different elements (Widlowski et al. 2006). Submeter spatial resolution imagery allows the extraction of pure crown pixels avoiding shadows and the tree crown edges that are more exposed to horizontal fluxes, therefore minimizing the effects of the canopy discontinuity. However, modelling the within-crown structural parameters remains a challenge when simulating tree crowns as a turbid medium. It has been demonstrated that the shaded gaps and the signal and angular arrangement of the different canopy elements including branches and twigs play an important role on the overall reflectance signal (Cescatti 1997; Verrelst et al. 2010). Regardless the limitations, 1D models have been

successfully inverted to retrieve complex canopy properties in the past (see Jacquemoud et al. (2009) for a review).

Here we show how SCOPE model inversion can be used to track photosynthetic activity in an almond tree orchard using high spatial resolution imagery collected with an airborne lightweight hyperspectral sensor. Although both the green and the red-far red spectral regions are explored, we show the potential of the green region to estimate $V_{c_{max}}$ for photosynthetic rate monitoring. The validity of the method is tested for independent datasets acquired at different phenological stages.

2. Materials and methods

2.1. Study site and experimental field

The study site is an almond orchard (cv. Guara onto GF-677 root-stock) located in Cordoba Spain (37°52'N, 4°49' W) growing under a Mediterranean weather characterized by warm and dry summers, cold and wet winters and an annual rainfall around 550 mm, mainly occurring in Spring and Autumn. The orchard was established in 2009 on a sandy loam soil in a 6 × 7 m grid, resulting in a tree density of 238 trees per ha.

During three years, four replicates of three different water and nutrient management treatments were applied to plots of 16 trees resulting in a wide range of stress variability. The first treatment, which trees were considered as control, was fertilized and irrigated to satisfy full requirements calculated following Fereres et al. (2012). The other two treatments followed a regulated deficit irrigation scheme (RDI), receiving 20% of full water requirements during kernel filling and 60% of control rates after harvest. The first of the RDI treatments received the same amount of N as the control treatment, fertilization rate of the second RDI was reduced to a 75% of the control. All trees were kept free of weeds, and pests and diseases were fully controlled. Table 1 gives an overview of the different treatments applied and a full description of the experimental site can be found in Espadafor et al. (2017) and Lopez-Lopez et al. (2018).

During the growing season, two central trees of each plot were monitored. Data collection included assimilation rate using a portable photosynthesis system (LCDpro-SD, ADC, Bioscientific Ltd., Herts, UK) and stomatal conductance with a porometer device (SC-1, Decagon Devices Inc., Pullman, WA, USA) both measured on two to four leaves per tree. Chlorophyll concentration was measured on 10 to 15 leaves using a SPAD meter (SPAD502DL, Minolta, Japan) and leaf steady-state fluorescence with a pulse amplitude modulated fluorometer (Fluorpen FP110, Photon Systems Instruments, Brno, Czech Republic) on 10 leaves per tree.

2.2. Field data collection and airborne campaigns

Two airborne campaigns were conducted using a nano-hyperspectral imager (Headwall Photonics, Fitchburg, MA, USA) on DOY: 218 and DOY: 237 (summer, 2015) corresponding to the kernel filling period and after harvest respectively. Flight design and airborne operations were

Table 1

Summary of irrigation and fertilization treatments applied in the experimental site.

Treatment	Irrigation	Fertilization
Treatment 1: Control	Full ET	100% N
Treatment 2: RDI 1	Regulated Deficit Irrigation: - 20% full ET during kernel filling - 60% after harvest	100% N
Treatment 3: RDI 2	Regulated Deficit Irrigation: - 20% full ET during kernel filling 60% after harvest	75% N

coordinated by the Laboratory for Research Methods in Quantitative Remote Sensing (QuantaLab) of the Consejo Superior de Investigaciones Científicas (IAS-CSIC, Córdoba, Spain). The specifications of the nano-hyperspectral imager used are detailed in Table 2. Flying operation was carried out on the solar principal plane at 250 m above ground level with a speed of 130 km/h, yielding a ground spatial resolution of 30 cm. Within 3 days of the image acquisition, a field dataset was collected by sampling two central trees of each treatment block as described above.

The imagery was radiometrically calibrated keeping the original instrument FWHM of 6.5 nm. Image raw data were transformed into radiance using calibration coefficients derived from measurements against a calibration standard (CSTM-USS-2000C LabSphere, North Sutton, NH, USA) at four integration times over four illumination intensities. The image atmospheric correction was conducted with SMARTS model (Gueymard 1995, 2002) using aerosol optical parameters measured with a handheld sun-photometer (Microtops II, Solar Light Co., Philadelphia, PA, USA) and air temperature, relative humidity and air mass measured with a portable weather station (WX510 from Vaisala, Vantaa, Finland).

Irradiance was also measured in the field with a cosine receptor unit attached to an upward looking spectrometer covering the 350–2500 nm spectral range (Fieldspec III Pro, Analytical Spectral Devices, Inc., Malvern Analytical, Malvern, UK). This field measured irradiance was later used as input in the model simulations. Ortho-rectification of each single hyperspectral flightline was performed using PARGE software package (ReSe Applications Schläpfer, Wil, Switzerland) based on the readings of an Inertial Measuring Unit (IMU) installed on-board the airborne platform during the flight.

The pixels corresponding to each individual tree crown in the orchard were selected using an automated process as reported in Calderon et al. (2015), ensuring only pure vegetation pixels were considered for the analysis. Fig. 1c presents an example of reflectance and radiance resulting from the segmentation for one tree crown from a control plot together with the irradiance measured at the time of the image acquisition. Fig. 2 shows the average reflectance and radiance spectra for the different treatments.

Spectral indices traditionally used for vegetation stress detection were calculated using the average value of the reflectance spectra extracted from each tree crown in the experiment (Table 3). The index selection comprises structural indices typically related to vigour and foliage density, indices used to assess pigment concentration and special attention was put on stress indices calculated from the green spectral region due to their connection to photoprotective processes under water and nutrient stress conditions. Sun-induced fluorescence was also retrieved from the hyperspectral imagery using the FLD principle applied to the O₂-A absorption line at 760 nm. The method was applied to the image data using the bands at 762 nm and 750 nm as the centre of the absorption feature and reference radiance, respectively (Table 3).

All spectral indices including FLD as an indicator of sun-induced

Table 2

Platform and sensor operational settings during image acquisition.

Hyperspectral sensor characteristics and settings	
Spectral range (nm)	400–885
Number of spectral bands	260
FWHM	6.5 nm
Slit size	25 μm
Detector pixel pitch	7.4 μm
Focal length	4.8 mm
Radiometric resolution (bits)	12
Integration time	18 ms
Image acquisition details	
Acquisition dates and times	6th & 25th August 2015, solar noon
Flying height (AGL)	250 m
Cruise speed	130 km/h
Mean spatial resolution (m)	0.3

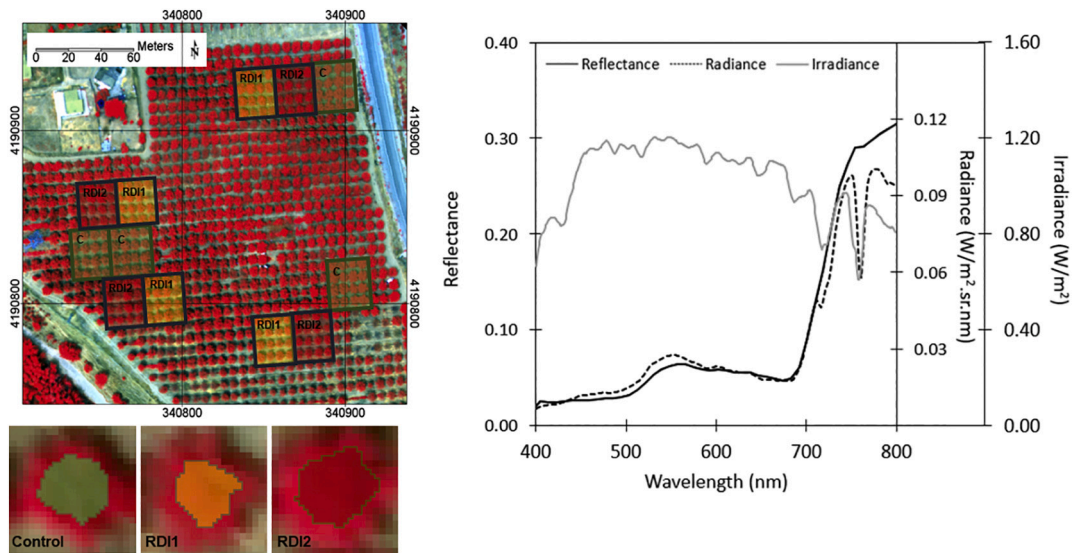


Fig. 1. Overview of the image captured over the experimental field on DOY 160 (a) with the control blocks in green (C), RD1 blocks in yellow and RD2 blocks in red. Zoom of the automatic segmentation applied to one tree of each treatment (b), example reflectance and radiance spectrum from a tree of the control group (c). (For interpretation of the references to colour in this figure legend, the reader is referred to the web version of this article.)

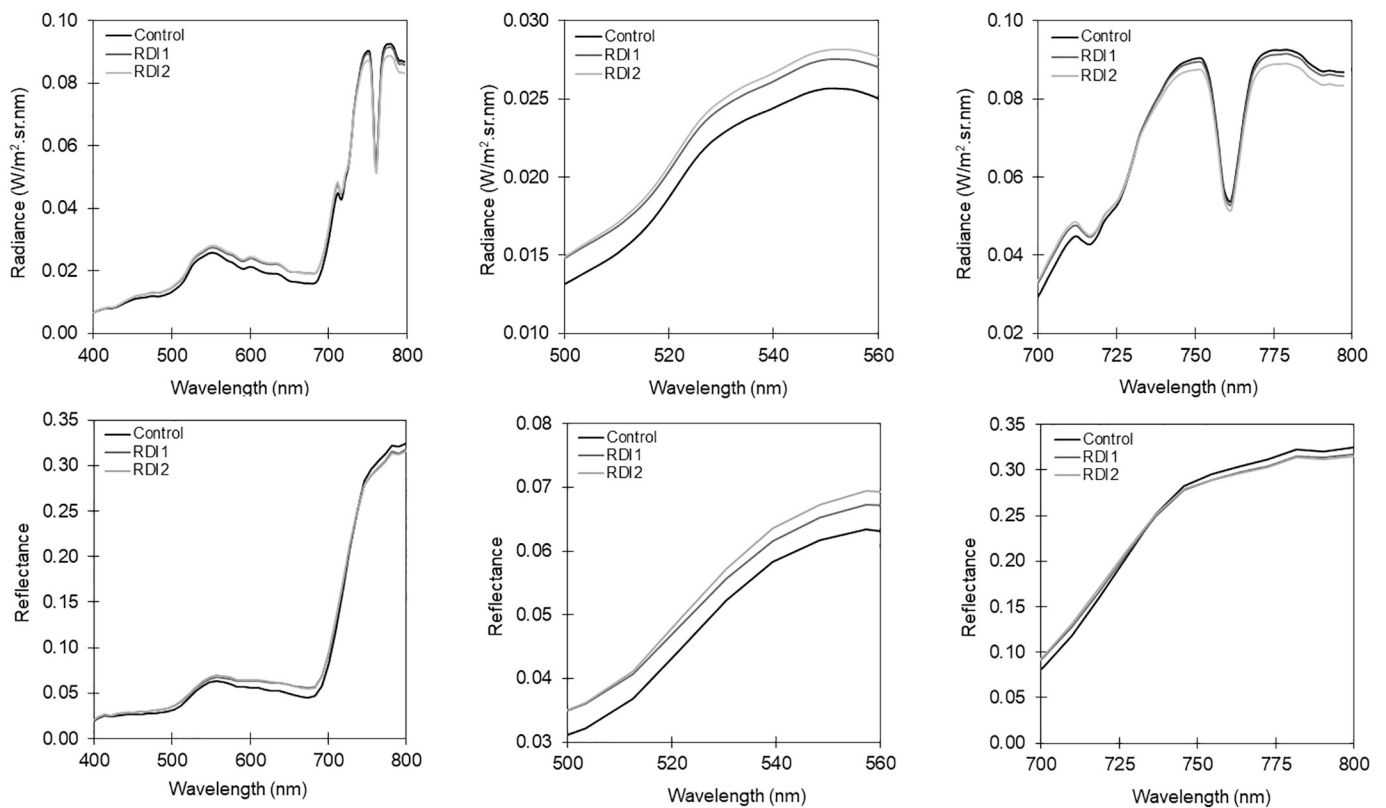


Fig. 2. Average radiance and reflectance spectrum for each of the treatments over the 400-800 nm spectral range (a and d), zooms over the green (500-560 nm) region (b and e) and far-red-NIR (700-800 nm) region (c and f) where physical models indicate $V_{c_{max}}$ change effects. (For interpretation of the references to colour in this figure legend, the reader is referred to the web version of this article.)

fluorescence were computed using the average reflectance and radiance extracted from each tree crown, being the tree crown our individual object of study. Linear interpolation was used to derive the reflectance value corresponding to each band in the formulas.

2.3. Simulation of $V_{c_{max}}$ spectral effects with SCOPE model

The SCOPE (Van der Tol et al. 2009) radiative transfer model (version 1.73) was used to simulate the effects of the photosynthetic performance changes on the canopy spectral signal, including the emitted chlorophyll fluorescence. SCOPE model incorporates the influence of photosynthetic activity processes into a coupled leaf-canopy

Table 3

List of spectral indices used in the study with their formulation and original reference. R_{λ} , L_{λ} and E_{λ} refer to reflectance, radiance and irradiance at λ nm.

Index	Formulation	Reference
Structural indices		
NDVI	$(R_{800} - R_{670}) / (R_{800} + R_{670})$	Rouse et al. (1973)
RDVI	$(R_{800} - R_{670}) / (R_{800} + R_{670})^{0.5}$	Rougean and Breon (1995)
EVI	$2.5 \cdot (R_{800} - R_{670}) / (R_{800} + 6 \cdot R_{670} - 7.5 \cdot R_{400} + 1)$	Huete et al. (2002)
MTVI	$1.2 \cdot (1.2 \cdot (R_{800} - R_{550}) - 2.5 \cdot (R_{670} - R_{550}))$	Broge and Leblanc (2000); Haboudane et al. (2004)
Chlorophyll indices		
CI	R_{750} / R_{710} $3 \cdot ((R_{700} - R_{670}) - 0.2 \cdot (R_{700} - R_{550}) \cdot (R_{700} / R_{670})) / ((1 + 0.16) \cdot (R_{800} - R_{670}) / (R_{800} + R_{670} + 0.16))$	Zarco-Tejada et al. (2001) Haboudane et al. (2002)
TCARI/OSAVI	$(R_{800} - R_{445}) / (R_{800} + R_{680})$	Peñuelas et al. (1995)
Xanthophyll-related Indices in the green region		
PRI	$(R_{570} - R_{530}) / (R_{570} + R_{530})$	Gamon et al. (1992)
PRI ₅₁₅	$(R_{515} - R_{530}) / (R_{515} + R_{530})$	Stagakis et al. (2012)
PRI _{M1}	$(R_{512} - R_{531}) / (R_{512} + R_{531})$	Gamon et al. (1993)
PRI _{M2}	$(R_{600} - R_{531}) / (R_{600} + R_{531})$	Gamon et al. (1993)
PRI _{M3}	$(R_{670} - R_{531}) / (R_{670} + R_{531})$	Gamon et al. (1993)
PRI _n	$PRI / [RDVI \cdot (R_{700} / R_{670})]$	Zarco-Tejada et al. (2013a, b)
Fluorescence quantification		
Fraunhofer Line Depth (FLD)	$FLD = ((E_{750} \cdot L_{762}) - (E_{762} \cdot L_{750})) / (E_{750} - E_{762})$	Plascyk and Gabriel (1975)

radiative transfer model resulting in a tool to study the effect of vegetation stress on the canopy reflectance. The leaf radiative transfer module is based on FLUSPECT-B leaf model (Wilfan et al. 2016) which simulates leaf reflectance using leaf thickness, dry matter and water content, chlorophyll, anthocyanin and carotenoid content. To incorporate the $V_{c_{max}}$ and J_{max} rates driving the RuBisCO enzyme activity in the photosynthetic process, the SCOPE model uses the Farquhar-von Caemmerer-Berry (FvCB; Farquhar et al. (1980)) photosynthesis model, the stomatal resistance (Cowan 1978), the Ball-Berry stomatal

conductance model (Ball et al. 1987) and the coupled photosynthesis-stomatal model by Collatz et al. (1991). $V_{c_{max}}$ and J_{max} determine the maximum carboxylation rate of RuBisCO and the maximum rate of photosynthetic electron transport varying in response to environmental conditions and governing the potential assimilation rate. J_{max} has been demonstrated to vary linearly with $V_{c_{max}}$ as function of air temperature (Woodward et al. 1995). The fluorescence and energy balance modules in SCOPE incorporate the effects of $V_{c_{max}}$ changes in the radiative transfer equation returning the overall canopy signal function of stress (Van der Tol et al. 2014). During its execution, the model ensures the energy balance closure integrating the thermal radiation, environmental conditions, leaf biochemistry and chlorophyll fluorescence and canopy radiative transfer (Van der Tol et al. 2009).

The SCOPE model input to track $V_{c_{max}}$ is the maximum carboxylation rate of a top leaf standardized to a reference temperature at 25 °C ($V_{c_{mo}}$). We will refer to it as $V_{c_{max}}$ from now onwards for easiness, and considering the air temperature at the time of image acquisition was within 5 degrees of the optimal 25 °C. The spectral effects resulting from varying $V_{c_{max}}$ can be seen Fig. 3, which shows the simulated spectra for $V_{c_{max}}$ changing from 0 to 250 $\mu\text{mol m}^{-2} \text{s}^{-1}$ using a standard set of input values and the ambient conditions at the time of DOY 237 airborne data collection. The effect on the signal is very subtle (dotted line, Figs. 3a-c) concentrated in the green region (505–560 nm) and in PS-I and PS-II chlorophyll fluorescence emission regions (650–800 nm). Fig. 3b and c show a zoom over the areas where this effect is observed. The same effects on the chlorophyll fluorescence emission region where reported by Zarco-Tejada et al. (2013a) using FluorSAIL radiative transfer model (Verhoef, 2005) coupled to FLIM (Rosema et al. 1992) developing the FluorFLIM hybrid model.

The absolute reflectance difference resulting from $V_{c_{max}}$ variation from 0 to 250 $\mu\text{mol m}^{-2} \text{s}^{-1}$ has similar dimensions in both the green and the fluorescence emission region (Fig. 3a, dotted line). The reflectance difference to reflectance signal ratio is therefore up to ten times higher in the green region than in the NIR as the reflectance in the visible is much lower as a result of pigment absorption. Fig. 3d represents the family of 200 simulations with $V_{c_{max}}$ ranging from 0 to 250 $\mu\text{mol m}^{-2} \text{s}^{-1}$ in the green region.

SCOPE simulations were also used to investigate potential

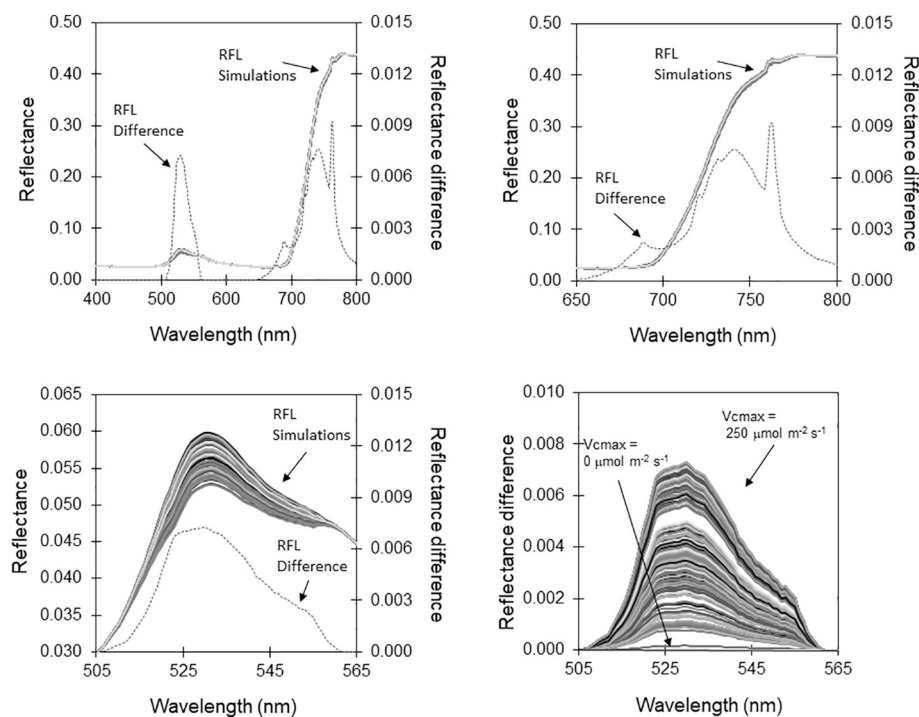


Fig. 3. Results of simulating the spectral response to $V_{c_{max}}$ variation over the range 10 to 250 $\mu\text{mol m}^{-2} \text{s}^{-1}$ leaving the rest of parameters fixed (LAI = 3, Cab = 80, Cm = Cw = 0.02) for the full 400–800 nm range (a), for the 650–800 nm region (b) and for 505–565 nm region (c). Reflectance difference between the maximum and minimum feature result of $V_{c_{max}}$ variation is represented in a dotted line. (d) reflectance difference represented for 200 simulations with $V_{c_{max}}$ ranging from 0 to 250 $\mu\text{mol m}^{-2} \text{s}^{-1}$ over the green spectral feature. (For interpretation of the references to colour in this figure legend, the reader is referred to the web version of this article.)

relationships between $V_{c_{max}}$ and existing indices in the green region (i.e. the Photochemical Reflectance Index (PRI), Gamon et al. (1992) and the family of formulations derived from PRI in Table 3) and SIF@760 quantified through the FLD method. $V_{c_{max}}$ vs PRI and $V_{c_{max}}$ vs SIF were investigated for chlorophyll content between 20 and 70 $\mu\text{g}/\text{cm}^2$ and for changes in LAI 1–2 to assess the potential of establishing links between vegetation indices and $V_{c_{max}}$ that are robust to variations in pigment content and vigour.

2.4. SCOPE model inversion for $V_{c_{max}}$ estimation

SCOPE model was inverted to retrieve $V_{c_{max}}$ as a proxy of assimilation rate for every tree in the experimental field acquired by the hyperspectral imager at the two acquisition dates. Please refer to the Appendix (Table A1) for specific SCOPE modules used. Inversions were carried out using pure vegetation pixels extracted without edge effects, as described previously. The model inversion was conducted based on the local spectral signal variations in the green (505–560 nm, as shown in Fig. 3c) and red-far red (690–750 nm, Fig. 3b) regions. In addition to using each region independently, the analysis also comprised both regions together and the full spectrum from 500 to 750 nm. Fig. 4 presents an overview of the steps followed to retrieve $V_{c_{max}}$ through model inversion.

Simulations were carried out with the atmospheric and background input parameters fixed according to known data or measurements on the image acquisition day. That includes location and sensor geometry, irradiance at the time of the flight, meteorological parameters and the soil reflectance. The irradiance used in the atmospheric module of SCOPE corresponded to the field-measured irradiance, while the direct and diffuse components were calculated to keep the modelled proportional contribution. As most of the canopy spectrum over the visible and NIR is the result of structure and pigment concentration, ill-posed solutions are frequent when those inputs are not well constraint and the parameter of interest has a comparatively small effect on the signal (Combal et al. 2003; Atzberger and Richter 2012). Consequently, a

multi-step inversion approach (Combal et al. 2001; Atzberger 2004; Laurent et al. 2014) was adopted to estimate $V_{c_{max}}$. First, model input parameters were constrained to specific ranges to avoid potential ill-posed inversion solutions. The ranges were established based on field measurements, existing literature and preliminary model simulations to make sure the resulting look-up-table (LUT) covered the tree crown spectral range of variability.

Under the assumption that in a well-managed orchard most structural properties present limited variation, the first inversions focused on fixing the ranges for the leaf structural parameter N and the leaf area index (LAI). Leaf orientation function was left to vary as it was demonstrated that almond trees adjust the leaf exposure to incoming illumination as function of stress (Egea et al. 2012). Leaf dry matter and water content are typically only affected after long term stress. In this case, they were also left to fully vary to consider the potential effect of long-term running treatments on the trees. Where there was not prior information or measurements, default values suggested for SCOPE model were used. Once the input ranges were established, the LUT was built by simulating a combination of random variations of the input values within the selected ranges. Table 4 shows the final input parameter ranges used to build the LUTs to invert $V_{c_{max}}$ for each image acquisition date. All simulations were convolved to the wavelength range, spectral sampling interval and FWHM of the nano-hyperspectral imager used in this study. The convolution was carried out assuming gaussian band spectral response functions of 6.5 nm FWHM centered at the imager band locations. After applying the spectral convolution to the simulated reflectance, both simulations and imagery spectral dataset were comparable to execute the inversion.

In order to remove data noise affecting model inversion and considering the bell-shaped response of changes in $V_{c_{max}}$ as opposed to narrow spectral features (Fig. 3), further smoothing of the data was applied using a low-degree polynomial filter (Savitzky and Golay 1964). The Savitzky-Golay filter was applied to the data on the whole spectral range excluding the region between 745 and 775 nm to avoid an impact on the O₂-A absorption region at 760 nm. For both simulations and

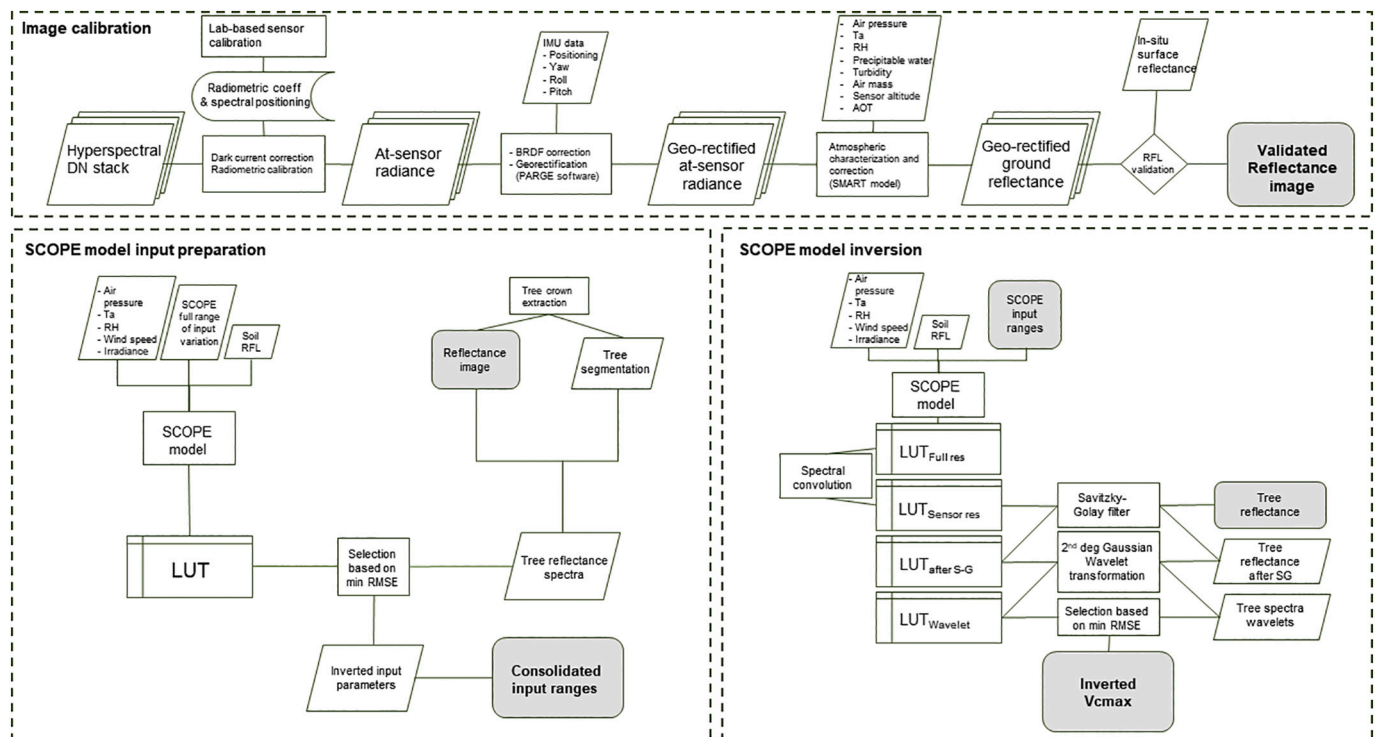


Fig. 4. Overview of the methodology used to retrieve $V_{c_{max}}$ through SCOPE model inversion including hyperspectral image calibration, SCOPE parametrisation and input preparation and SCOPE model inversion.

Table 4
Input units and intervals used for SCOPE model inversion.

Parameter	Definition	Unit	Range / Value
Leaf biophysical parameters			
N	Leaf structural parameter	[-]	1.7–1.9
C _{ab}	Chlorophyll a & b content	µg/cm ²	35–60
C _{car}	Carotene content	µg/cm ²	6–18
C _{ant}	Anthocyanin content	µg/cm ²	0–8
C _w	Leaf water content	g/cm ²	0.001–0.05
C _m	Leaf dry matter content	g/cm ²	0.001–0.05
C _s	Brown pigment content	µg/cm ²	0
lw	Leaf width	m	0.07
Leaf biochemistry			
V _{cmax}	Maximum carboxylation rate	µmol/m ² ·s	30–110
m	Ball-Berry stomata conductance	[-]	8
R _{dparam}	Dark respiration	[-]	0.015
K _v	Vertical profile of V _{cmax} extinction coefficient	[-]	0.64
K _c	Cowan's water use efficiency	[-]	700
T	Temperature sensitivity parameters for V _{cmax} and Resp	[-]	0.2, 0.3, 283, 311, 328
ρ(thermal)	Leaf reflectance in thermal region	[-]	0.01
τ(thermal)	Leaf transmittance in thermal region	[-]	0.01
ρ _s (thermal)	Soil reflectance in thermal region	[-]	0.06
Stressfactor	Stress impact on V _{cmax}	[-]	1
f _{qe}	Fraction of photons partitioned to PSII	[-]	0.02
Canopy parameters			
LAI	Leaf area index	m ² / m ²	0.5–2.3
LIDF _a	Leaf Inclination Distribution Function parameter a	[-]	-0.5–0.5
LIDF _b	Leaf Inclination Distribution Function parameter b	[-]	-0.5–0.5
Micrometeorological			
p	Air pressure	hPa	1010
u	Wind speed	m/s	1.6
O _a	O2 concentration in the air	ppm	209
ea	Atmospheric vapour pressure	hPa	0.15
C _a	CO2 concentration in the air	ppm	380
T _a	Air temperature	°C	30
R _{in}	Incoming shortwave radiation	W/m ²	700
R _{li}	Incoming longwave radiation	W/m ²	300

image data, the amplitude of the second degree gaussian wavelet transformation was computed over four spectral ranges: i) 505–560 nm; ii) 690–750 nm, iii) the combination of both; and iv) the full 500–750 nm range. V_{cmax} was estimated for each tree crown as the LUT entry with closest wavelet transformed spectrum using the root mean square error as cost function [1]. The rest of the input parameters derived for each tree crown were used for verification purposes only (e.g. to validate the consistency of the results over time).

$$RMSE = \sqrt{\frac{\sum_{\lambda_i}^{\lambda_j} (Wa_{obs}(\lambda) - Wa_{sim}(\lambda))^2}{N}} \quad (1)$$

Where λ_i and λ_j are the initial and end band of the spectral range, N is the total number of bands and $Wa_{obs}(\lambda)$ and $Wa_{sim}(\lambda)$ are the wavelet amplitude from the image and from the model simulations, respectively, at a specific wavelength.

Similar method was applied by Kattenborn et al. (2017) to derive plant traits from airborne hyperspectral imagery. The only adaptation made in this study was to include only 3 scales in the wavelet transformation. The reason to use less scales was to adjust the width of the wavelets to inform the changes over smaller spectral regions as opposed to characterising the effects over the full visible-NIR spectral signal. Artifacts resulting from potential signal noise on those spectral regions were removed after applying the smoothing filter. A lower filter size was applied to the red-far red region to avoid the elimination of narrow

spectral effects.

3. Results

3.1. Field measurements

Physiological measurements collected in the field at the time of the image acquisitions depicted the stress variability consequence of the different water and nutrient management treatments. The ranges of variation of the leaf data collected on the whole experiment are shown in Fig. 5.

Leaf assimilation rates varied from 1.2 to 16.2 µmol m⁻² s⁻¹ for all the leaves measured. The measurements were averaged per tree and later per treatment plot (2 trees per plot) for a total of 4 repetitions per treatment. Averaged plot values were used for further analysis. The ranges of variation found for the rest of the leaf parameters measured in the field can be found in Figs. 5b-d.

The impact of varying LAI and chlorophyll content on the spectra, and therefore on the relationships V_{cmax} vs. PRI and V_{cmax} vs. SIF was further investigated using SCOPE simulations. Fig. 6 shows there is not a single relationship for V_{cmax} estimation using PRI or SIF as the relationship is highly affected by the canopy structure (i.e. LAI; Fig. 6a and b) and chlorophyll content (Fig. 6c and d). Similar results were obtained for other indices of the PRI family developed to account for the effects of canopy structure or pigment concentration (data not shown).

3.2. SCOPE model inversion for V_{cmax} estimation

The lack of a single relationship between modelled V_{cmax} and PRI, highly affected by structure and chlorophyll content, explains why the coefficients of determination and significance of the relationships between reflectance indices calculated from the hyperspectral imagery and the field-measured assimilation rate for each day are not very strong, ranging between r² = 0.04 and r² = 0.47. Still, indices in the green region and FLD as a proxy of SIF outperformed structural and pigment indices when tracking assimilation levels (Table 5).

V_{cmax} derived from model inversion using the green spectral region presented more robust relationships vs. assimilation rates measured in the field for both days than those obtained from the reflectance indices described above (r² = 0.67–0.84, p-value < 0.005). The relationships between V_{cmax} and assimilation showed a steady increasing trend until reaching a saturation around 100 µmol m⁻²·s⁻¹ (Fig. 7). The retrieved parameter ranges resulting from the model inversion fell within expected ranges and have been included in the Appendix for reference together with and a comparison of the inverted and image spectrum for one monitored tree per treatment (Figs. A1 and A2 respectively). The results of applying the same model inversion method to other spectral regions did not yield as good results (Table 5).

V_{cmax} retrieved by model inversion showed higher maximum carboxylation rate for higher assimilation and overall better separability between treatments than commonly used vegetation indices (one-way ANOVA analysis p-value = 0.08 as opposed to p-value = 0.20–0.96; eta value indicating the proportion of the variance among groups that is explained by each factor η = 0.5 as opposed to η = 0.1–0.4) as it was estimated accounting for the structural differences across the experimental field (Fig. 8b).

Both SIF and PRI followed the general trend of the differences found in assimilation rates. As expected, treatment blocks with higher assimilation rates (Fig. 8a) also showed higher SIF in average (Fig. 8c) and lower PRI (Fig. 8d) corresponding to lower proportional content of photoprotective xanthophyll compounds. The means of both the Normalised Difference Vegetation Index (NDVI) and the Chlorophyll Index (CI) per treatment, indices developed to track vigour and chlorophyll changes, did not follow the trends of assimilation measured for each treatment as clearly as V_{cmax} (Fig. 8e and f).

The analysis of V_{cmax} derived from model inversion using the green

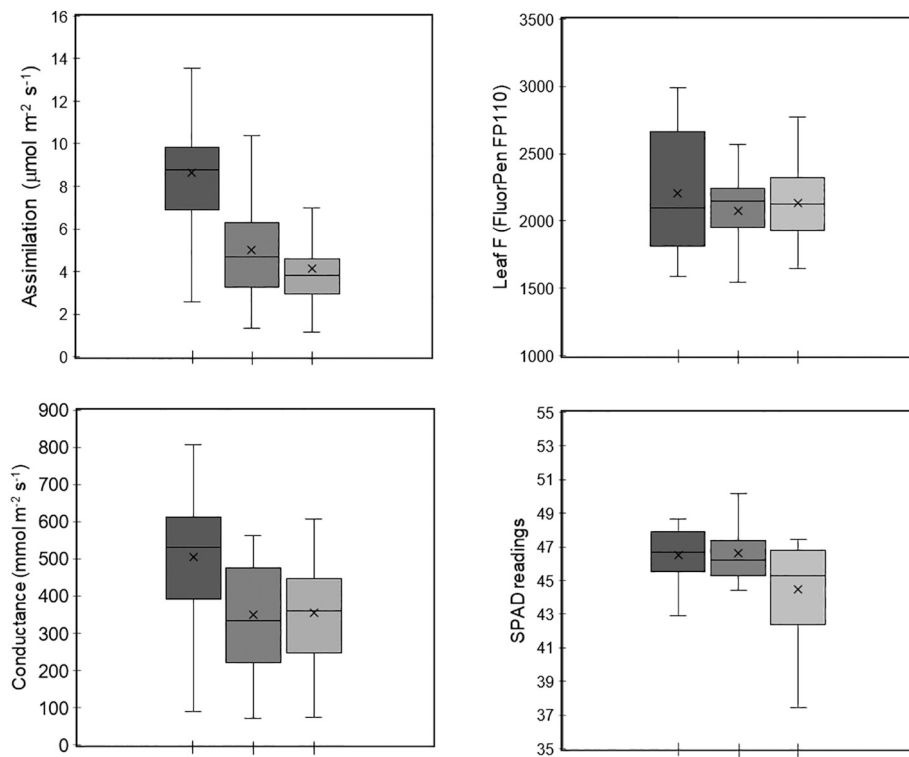


Fig. 5. Ranges of variation for the four physiological variables measured in the field at both dates: Assimilation rate (a), stomata conductance (b), steady-state fluorescence (c) and SPAD chlorophyll index (d). Crossing line refers to median value and box amplitude refers to the second and third quartiles' limits. Whiskers represent the max and minimum data without outliers.

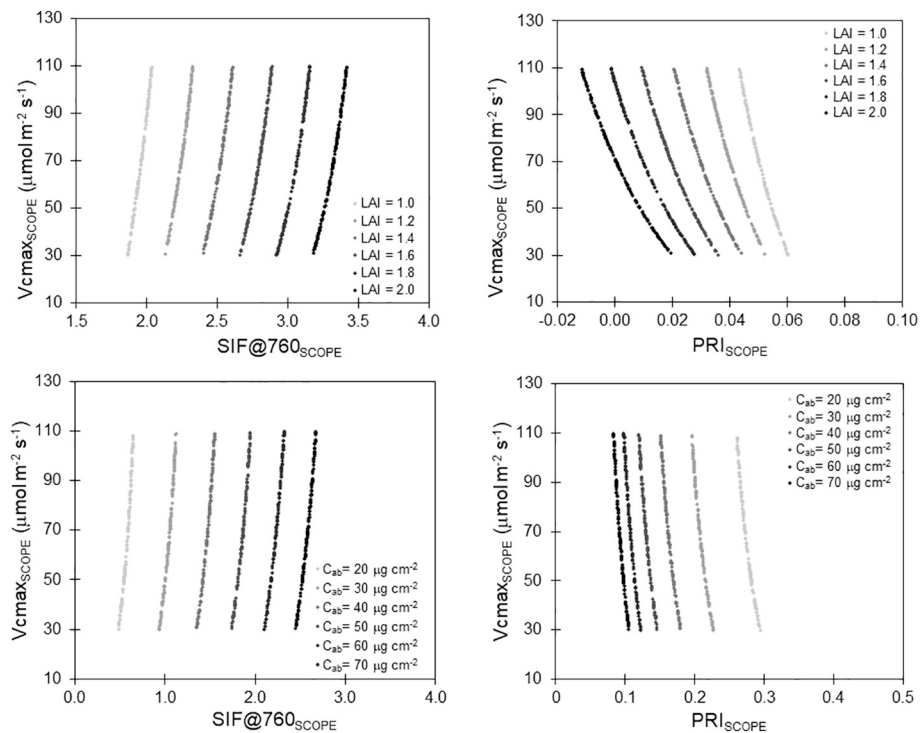


Fig. 6. Results of modelling the effect of chlorophyll content and LAI variation on $V_{c_{max}}$ vs sun-induced chlorophyll fluorescence calculated with the in-filling method at 760 nm (a and c) and $V_{c_{max}}$ vs PRI (b and d).

spectral region and A was shown to be more robust across dates, as displayed in Fig. 9a and Table 5. On the other hand, SIF and PRI did not follow the same trend when both dates were analysed together, being

highly affected by environmental conditions and illumination at the moment of the data capture. NDVI presented more stability over time although, as it is a proxy of tree vigour and only indirectly linked to

Table 5

Coefficients of determination (r^2) for the relationships between assimilation vs. the different vegetation indices and vs. $V_{c_{max}}$ resulting from SCOPE model inversion using wavelet transforms over 4 different spectral regions.

Index	r^2 (DOY: 218)	r^2 (DOY: 237)	r^2 (both days)
Structural indices			
NDVI	0.38*	0.27*	0.25*
RDVI	0.38*	0.15	0.18*
EVI	0.39*	0.16	0.20*
MTVI	0.37*	0.16	0.13*
Chlorophyll indices			
CI	0.35*	0.13	0.27*
TCARI/OSAVI	0.15	0.04	0.11
SIPI	0.37*	0.05	0.23*
Indices based on the green region			
PRI	0.44*	0.32*	0.17*
PRI ₅₁₅	0.41*	0.19	0.26*
PRI _{M1}	0.42*	0.18	0.26*
PRI _{M2}	0.47*	0.34*	0.24*
PRI _{M3}	0.41*	0.27*	0.21*
PRI _n	0.42*	0.33*	0.26*
Fluorescence indicators			
FLD	0.49*	0.64**	0.35*
$V_{c_{max}}$ from SCOPE model inversion			
505–560 nm	0.67**	0.84***	0.56***
700–750 nm	0.41*	0.25	0.16*
505–650 nm & 700–750 nm	0.47*	0.09	0.12
500–750 nm	0.38*	0.05	0.21*

* p-value < 0.1.

** p-value < 0.01.

*** p-value < 0.001

assimilation rate, it did not show a strong relationship as $V_{c_{max}}$ derived by model inversion.

4. Discussion

According to the radiative transfer modelling analyses carried out to study the effects of $V_{c_{max}}$ on the electromagnetic spectrum, the spectral regions that are affected by $V_{c_{max}}$ changes are located in the green over the 505–560 nm range and in the red-far red region between 650 and 800 nm, where chlorophyll fluorescence is emitted. This analysis is in agreement with the results obtained assessing different hyperspectral reflectance indices, which show stronger correlations between assimilation rates measured in the field and spectral indices based on green bands such as the Photochemical Reflectance Index (PRI) (Table 5) and

SIF. It also suggests that those are the regions that need to be used to retrieve $V_{c_{max}}$ through model inversion using SCOPE.

There is extensive literature that focuses on using the green and the chlorophyll fluorescence regions to detect pre-visual vegetation stress, that is, before changes are detectable by structural indices (Peñuelas et al. 1994; Thenot et al. 2002; Suarez et al., 2009; Flexas et al. 2000, 2002; Moya et al. 2004; Perez-Priego et al., 2005) and photosynthetic performance (Filella et al. 1996; Trotter et al. 2002; Evain et al. 2004). However, it has also been demonstrated that PRI indices are highly affected by illumination geometry, vegetation structure, pigment composition and soil background (Barton and North 2001; Suarez et al., 2008), making their application over large areas challenging. Here we also show with physical modelling that the effects of LAI and chlorophyll content variations prevent PRI and SIF indices from having a direct universal link to assimilation rates (Fig. 6). In addition to this, the methods using the PRI family of indices or SIF over time series require normalisation techniques to account for the differences in illumination intensity at the time of image acquisition (Suarez et al., 2010; Zarco-Tejada et al. 2016) or within field structural or biophysical heterogeneity (Zarco-Tejada et al. 2013b; Koffi et al. 2015). Hence, these reasons suggest that methods based on spectral indices would fail at representing the variability of assimilation rate over time in crops where long-term stress has had an impact on growth and leaf composition.

In the past, new formulations and normalisations were developed to track plant traits overcoming confounding effects like LAI or pigment content (see PRI derived indices in Table 3; Haboudane et al. 2002; Zarco-Tejada et al., 2013a, b; Woodgate et al. 2019). Still, these formulations end up being species specific and they need to be used in combination with empirical links to a particular trait. Established empirical relationships between vegetation indices and plant traits add another level of complexity as these relationships are highly empirical and difficultly transferable across fields and scales. The quantification of plant traits directly linked with plant functioning through physical model inversion allows vegetation monitoring precisely, being transferable and applicable over time series. In this study, we attempted the quantification of $V_{c_{max}}$ to track the limitation in photosynthetic efficiency under stress. The method accounts for varying LAI and leaf chlorophyll content parameters to overcome the limitations pointed out in Fig. 5 and the wide range of variation found in the field as a result of a long-term experimental design. We also assumed within-field variations in other pigments concentration, constituents and variations in leaf inclination distribution function which has demonstrated a very dynamic response to stress in almond trees (Egea et al. 2012). With SCOPE model we can simulate the effects of plant stress on the photosynthetic efficiency and the resulting reflectance signal under different illumination and ambient conditions (Van der Tol et al. 2014) ensuring the

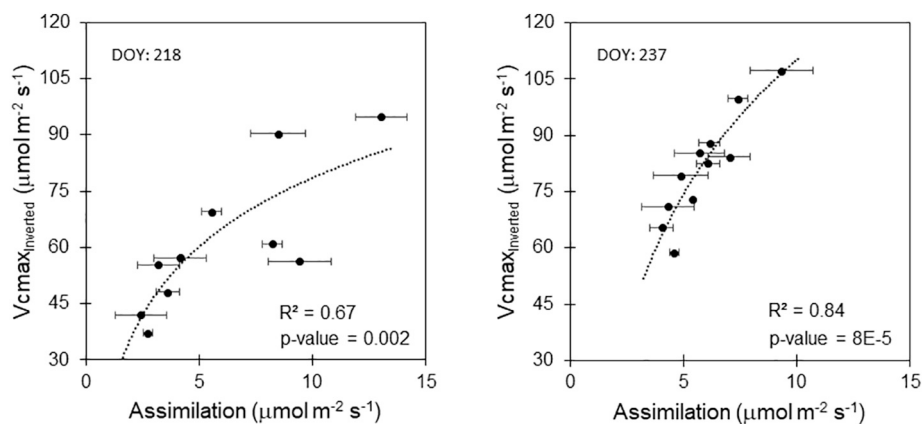


Fig. 7. Logarithmic relationships between $V_{c_{max}}$ derived from SCOPE model inversion using the 505–560 nm spectral region and assimilation rates measured in the field at both data acquisition dates DOY: 218 during kernel filling (a) and DOY: 237 after harvest (b). Error bars refer to standard deviation values for assimilation measurements in the field.

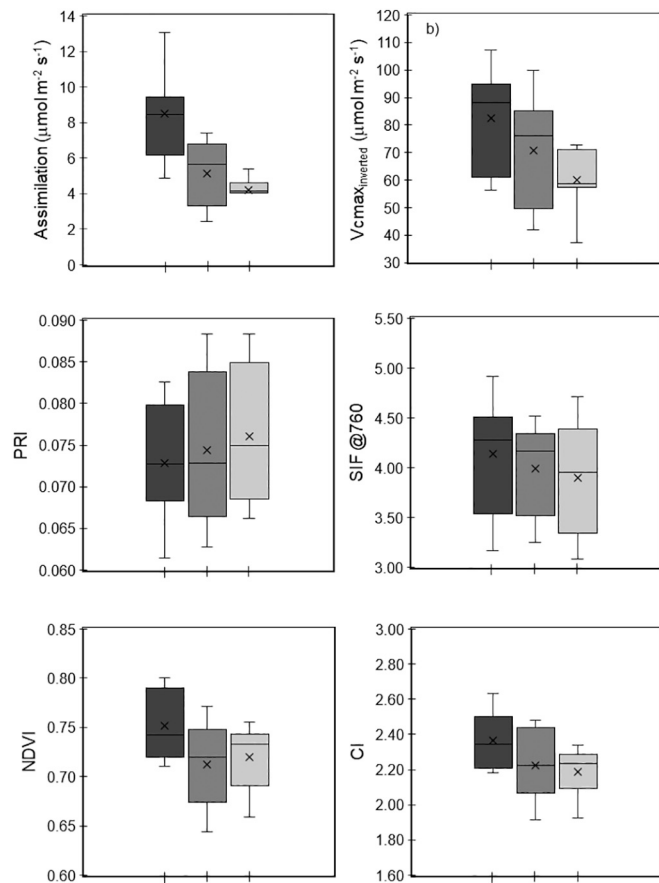


Fig. 8. Ranges of variation found in crown averages for each treatment for assimilation rate (a), $V_{c_{max}}$ inverted using SCOPE (b), PRI derived from the hyperspectral image (c) and SIF calculated from the image data using the infilling method at 760 nm O_2-A band (d). Crossing line refers to median value and box amplitude refers to the second and third quartiles' limits. Whiskers represent the max and minimum data without outliers and middle 'x' refers to the mean value.

applicability of the method to time series of data.

One limitation of SCOPE model is that the canopy radiative transfer module assumes a continuum 1D layer, lacking the capacity of other models that account for full 3D structural parametrization of tree crowns. Previous work has proved that the quantification of $V_{c_{max}}$ through SCOPE model inversion is achievable for wheat (Camino et al., 2019), a homogeneous single layer crop without woody elements and complex ramifications. Recent developments of SCOPE adapted the radiative transfer to account for the vertical heterogeneity of biophysical inputs across the canopy (Yang et al. 2017) but the capability of simulating tree crowns is still not present. Nevertheless, high-resolution imagery allows extracting crown spectra from pure vegetation pixels. We applied the model inversion to pure vegetation pixels and our results suggest that $V_{c_{max}}$ derived from model inversion can be used to track assimilation rates in orchard trees.

Inverting SCOPE to derive $V_{c_{max}}$ using the green spectral region yielded better results with field-measured assimilation rate ($r^2 = 0.7-0.8$) than any other approach based on common narrow-band spectral indices ($r^2 = 0.3-0.5$), SIF ($r^2 = 0.5-0.6$) or model inversion using other spectral regions (Table 5). Previous studies have inverted SCOPE to derive $V_{c_{max}}$ based on the SIF signal, these studies are either using satellite imagery with low spatial resolution (Zhang et al. 2014, 2018) or are applied to continuous crops lacking the complex architecture of woody canopies (Camino et al., 2019). Retrieving $V_{c_{max}}$ for individual crowns using SCOPE poses extra challenges related to the proper structural characterisation of the canopy with a model that does

not account for branching architecture and the presence of woody components. By employing the wavelet transformed amplitude, the estimations are resulting from the local variation of reflectance function of $V_{c_{max}}$ response feature. This technique removes the effects of wider spectral region variation while quantifying the narrow effects (Mittermayr et al. 2001) and has been suggested as a method to minimise the effects of canopy structure on the spectral signal (Blackburn 2006). Hence the technique is not as affected by errors in atmospheric corrections as if the inversion is based on the minimum spectral distance. This method has been used in the past to invert plant traits from hyperspectral imagery yielding similar results (Blackburn and Ferwerda 2008; Cheng et al. 2011; Kattenborn et al. 2017). The use of the green region as opposed to the chlorophyll fluorescence emission region has further benefits for future applicability of the method because 1) detectors have higher sensitivity over the visible part of the spectrum and the signal to noise ratio is higher, 2) there are not narrow atmospheric absorption features, ensuring a more reliable calibration regardless the quality of ancillary data measured in the field, 3) vegetation reflectance in the green region typically varies within a 5% and does not present abrupt changes driven by vegetation structure like in the red-far-red regions and 4) the absolute signal variation due to $V_{c_{max}}$ changes presents a higher proportional variation on the signal due to the higher absorption of light in the visible. On the other hand, in the green region there is a high absorption due to different photosynthetic pigments, and it is a region where their temporal dynamics is not yet well understood, in particular under stress conditions.

The results suggest that the inverted maximum carboxylation rate increases linearly with assimilation measured in the field up to a saturation point. At that point, around $100 \mu\text{mol m}^{-2} \text{s}^{-1}$, the maximum carboxylation rate is not limiting assimilation in a linear manner. Zarco-Tejada et al. (2016) found a similar trend between assimilation and SIF. This could be attributed to a non-linear relationship between assimilation and respiration as they are known to respond differently to environmental factors like temperature (Bowling et al. 2001; Knohl and Buchmann 2005) and stress (Raggi 1995; Reichstein et al. 2005). Further SCOPE model analysis shows how the air temperature has an effect on the relationship between $V_{c_{max}}$ and assimilation (data not shown), this effect is still to be properly assessed in order to track assimilation rates for periods with highly changing environmental conditions. Another cause can be the potential variability of the $J_{max}/V_{c_{max}}$ ratio, which has been demonstrated to vary with leaf temperature in almond trees (Egea et al. 2011).

The common trend followed by the results of both data acquisition days ($p\text{-value} < 0.0001$) indicates this method is applicable to time series without the need of further normalisation providing a reliable tool to quantitatively track photosynthetic rate in tree orchards using SCOPE. Although previous studies have successfully track $V_{c_{max}}$ trends over time, these are limited to herbaceous crops over coarse spatial scales (Zhang et al. 2014). Previous methods also relied on the successful retrieval of SIF remotely, or require a high and accurate set of ancillary data (Guanter et al. 2014; Bayat et al. 2018). The results suggest the methodology presented in this study using the green spectral region properly accounts for existing biophysical variability and overcomes the confounding structural effects on the spectra while empirical models alone based on the same part of the spectrum could not fully track assimilation differences. Furthermore, this study demonstrates that it is possible to track photosynthetic efficiency with an ultralight hyperspectral sensor that can be flown on board unmanned platforms (Lucieer et al. 2014), opening several avenues of future research and applications in remote sensing science of plant functioning.

5. Conclusions

The remote assessment of photosynthetic performance under stress is challenging due to the confounding effects of varying structural and biophysical properties in woody crops such as in the case of orchards.

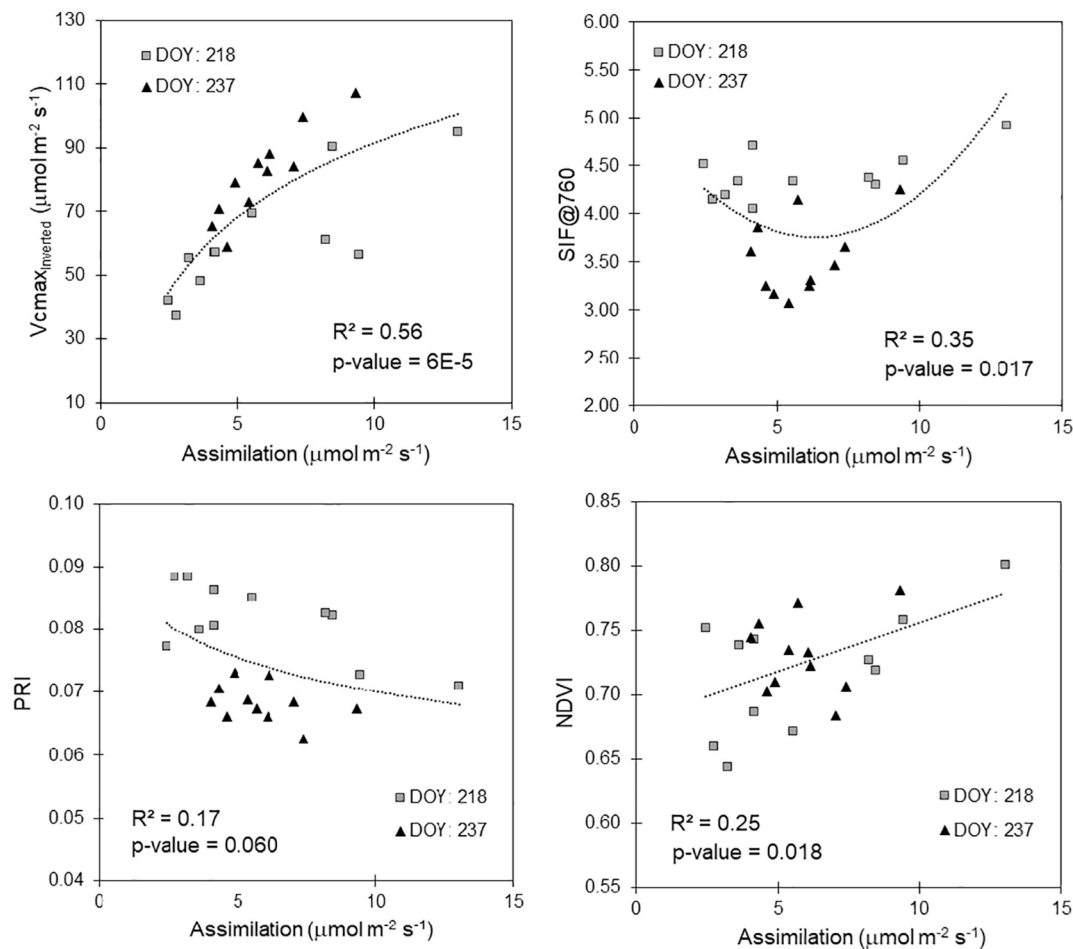


Fig. 9. Relationships obtained between assimilation rate measured in the field and $V_{c\max}$ derived from SCOPE model inversion using the green spectral region (a), SIF quantified from hyperspectral imagery through the FLD principle (b), PRI (c) and NDVI (d) spectral indices for all the measurements at kernel filling (DOY: 218) and at harvest (DOY: 237). (For interpretation of the references to colour in this figure legend, the reader is referred to the web version of this article.)

Here, we present a methodology that accounts for the variability in the structural and pigment composition to quantify the maximum carboxylation rate ($V_{c\max}$) as an indicator of photosynthetic rate reductions under stress through SCOPE model inversion. Results suggest that the methodology presented overcomes the biophysical and illumination effects while narrow-band spectral indices cannot fully assess assimilation differences across dates. The robustness of the method has been demonstrated with datasets acquired at two different times along the season. Finally, the lightweight specifications of the hyperspectral sensor used in this study allows its use from both manned and unmanned platforms, providing a flexible, affordable and practical means to both small and large area crop monitoring and assessment of plant functioning traits.

Credit author statement

PZT and LS conceived the idea. VGD, CC collected field data and provided background information, AH developed the sensor calibration and pre-processing chain, LS developed the method and analysed the data, LS and PZT wrote the manuscript, all authors helped reviewing and updating the manuscript.

Declaration of Competing Interest

The authors declare that they have no known competing financial interests or personal relationships that could have appeared to influence the work reported in this paper.

Acknowledgments

The experiment was carried out in the experimental farm "Alameda del Obispo" belonging to IFAPA. The authors gratefully acknowledge the financial support of the Spanish Ministry of Science and Education for projects AGL2012-40053-C03-01 and AGL2012-35196 and of the Regional Government of Andalusia, Spain, for project P12-AGR-2521. Ignacio Lorite and Elías Fereres are acknowledged for their support to this work. The authors would also like to thank R. Romero, D. Notario and A. Vera for their technical support during the airborne campaign and the image processing conducted in the QuantaLab-IAS-CSIC laboratory. M. López-López, M. Orgaz, K. Gutiérrez, and R. Luque are also acknowledged for their fieldwork in the almond orchard.

Appendix 1. SCOPE settings

Table A1

List of modules available in SCOPE v1.73 and their use for this study together with the definition provided by the model developer.

SCOPE v1.73 Module	Use (Y = 1/N = 0)	Module definition
calc_ebal	1	calculate the complete energy balance
calc_vert_profiles	0	calculate vertical profiles of fluxes and temperatures
calc_fluor	1	calculate chlorophyll fluorescence
calc_plank	0	calculate spectrum of thermal radiation with spectral emissivity instead of broadband
calc_directional	0	calculate BRDF and directional temperature for many angles specified in a file.
calc_xanthophyllabs	1	calculate dynamic xanthophyll absorption (zeaxanthin), for simulating PRI
calc_PSI	0	0 (recommended): treat the whole fluorescence spectrum as one spectrum, 1: differentiate PSI and PSII with Franck et al. spectra
rt_thermal	0	0: provide emissivity values as input. 1: use values from fluspect and soil at 2400 nm for the TIR range
calc_zo	0	0: use the zo and d values provided in the inputdata, 1: calculate zo and d from the LAI, canopy height, CD1, CR, CSSOIL (recommended if LAI changes in time series)
soilspectrum	0	0: use soil spectrum from a file, 1: simulate soil spectrum with the BSM model
soil_heat_method	0	0: standard calculation of thermal inertia from soil characteristics, 1: empirically calibrated formula (make function), 2: as constant fraction of soil net radiation
Fluorescence_model	0	0: empirical, with sustained NPQ (fit to Flexas' data); 1: empirical, with sigmoid for Kn; 2: Magnani 2012 model
calc_rss_rbs	0	0: use resistance rss and rbs as provided in inputdata. 1: calculate rss from soil moisture content and correct rbs for LAI
apply_T_corr	1	correct Vcmax and rate constants for temperature in biochemical.m
verify	0	verify the results (compare to saved 'standard' output) to test the code for the first time
save_headers	1	write header lines in output files
makeplots	0	plot the results
simulation	0	0: individual runs, 1: time series, 2: Lookup-Table

Appendix 2. SCOPE model inversion results

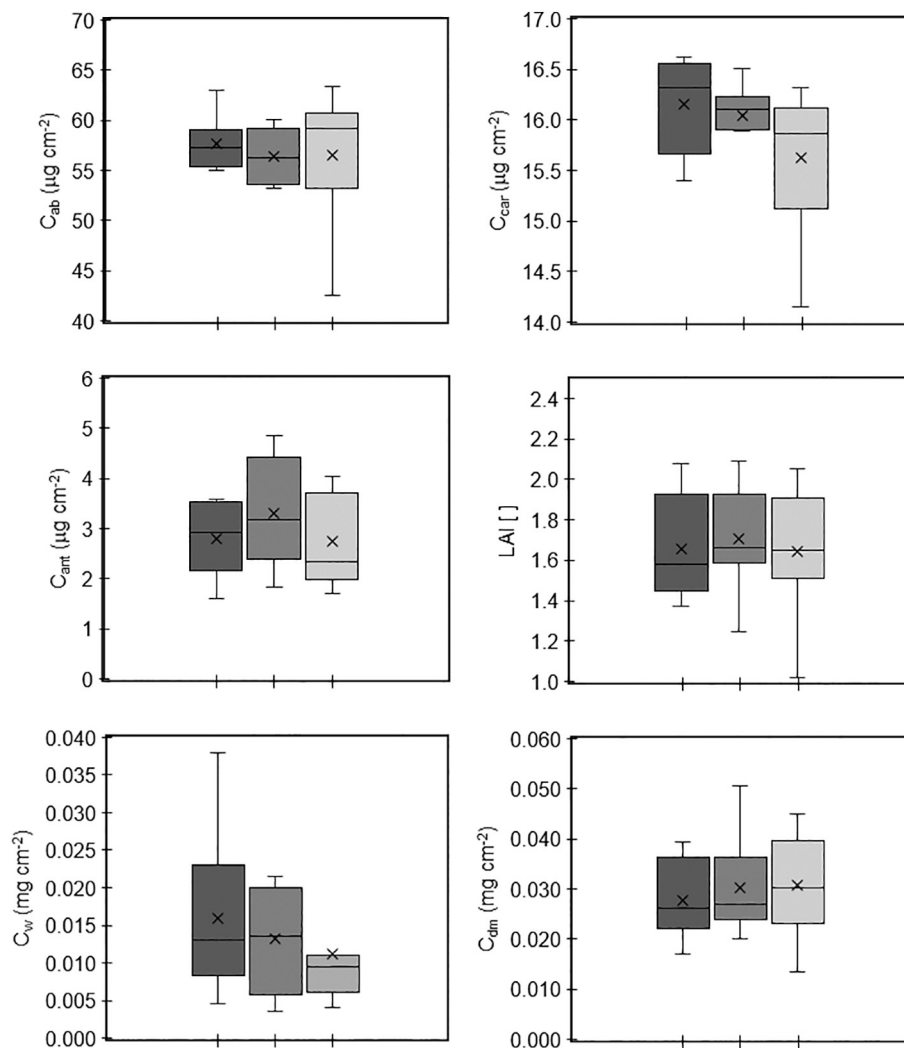


Fig. A1. Ranges of variation of SCOPE input parameter inversion for each treatment for chlorophyll (a), carotenoid (b), anthocyanin (c), LAI (d), water (e) and dry matter content (f). Crossing line refers to median value and box amplitude refers to the second and third quartiles' limits. Whiskers represent the max and minimum data without outliers and middle 'x' refers to the mean value.

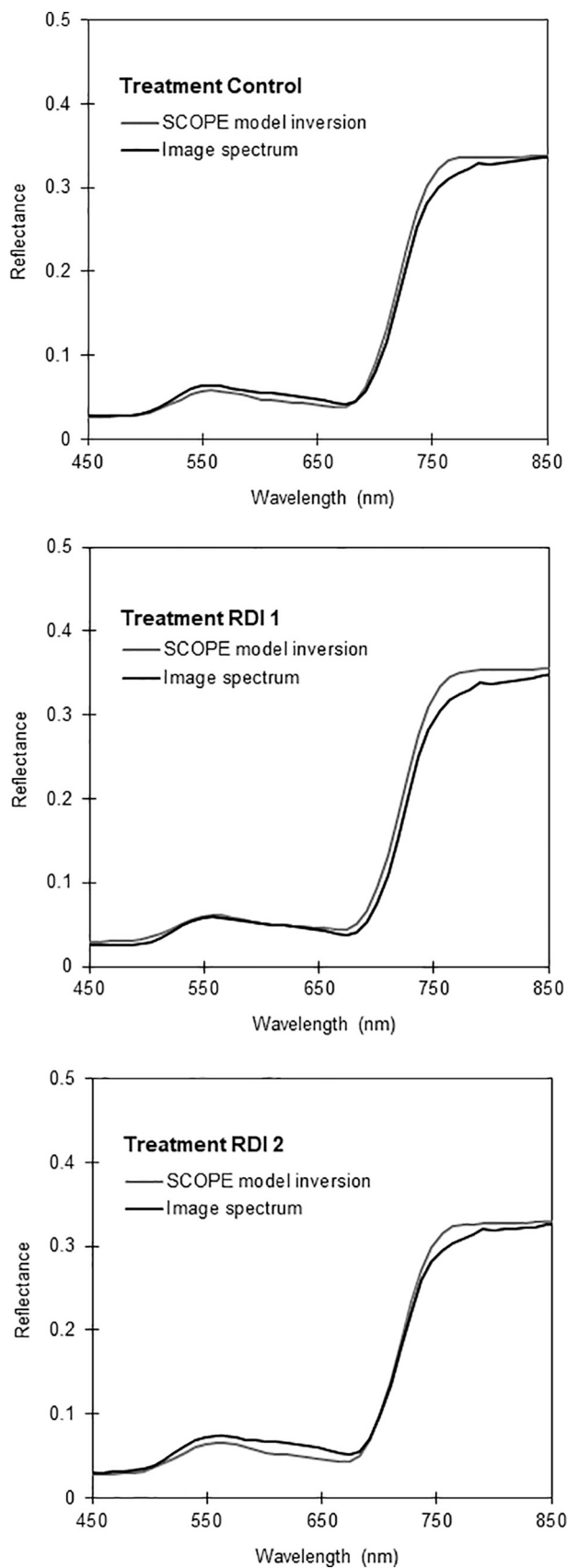


Fig. A2. Comparison of spectra obtained from SCOPE model inversion and image average spectra for one monitored tree per treatment: Control (a), RD11 (b) and RD12 (c).

References

- Verhoef, W., 2005. Extension of SAIL to model solar-induced canopy fluorescence spectra. In: 2nd International Workshop on Remote Sensing of Vegetation Fluorescence, 17–19 Nov. 2004, Montreal, Canada.
- Atzberger, C., 2004. Object-based retrieval of biophysical canopy variables using artificial neural nets and radiative transfer models. *Remote Sens. Environ.* 93 (1–2), 53–67.
- Atzberger, C., Richter, K., 2012. Spatially constrained inversion of radiative transfer models for improved LAI mapping from future Sentinel-2 imagery. *Remote Sens. Environ.* 120, 208–218.
- Ball, J.T., Woodrow, I.E., Berry, J.A., 1987. In: Biggins, J. (Ed.), *A Model Predicting Stomatal Conductance and its Contribution to the Control of Photosynthesis under Different Environmental Conditions BT - Progress in Photosynthesis Research: Volume 4 Proceedings of the VIII International Congress on Photosynthesis* Providence, Rhode Island, USA, August 10–15, 1986. Springer Netherlands, Dordrecht.
- Barton, C.V.M., North, P.R.J., 2001. Remote sensing of canopy light use efficiency using the photochemical reflectance index. Model and analysis. *Remote Sensing of Environment* 78 (264), 273.
- Bayat, B., van der Tol, C., Verhoef, W., 2018. Integrating satellite optical and thermal infrared observations for improving daily ecosystem functioning estimations during a drought episode. *Remote Sens. Environ.* 209, 375–394.
- Blackburn, G.A., 2006. Hyperspectral remote sensing of plant pigments. *J. Exp. Bot.* 58 (4), 855–867.
- Blackburn, G.A., Ferwerda, J.G., 2008. Retrieval of chlorophyll concentration from leaf reflectance spectra using wavelet analysis. *Remote Sens. Environ.* 112, 1614–1632.
- Bowling, D.R., Tans, P.P., Monson, R.K., 2001. Partitioning net ecosystem carbon exchange with isotopic fluxes of CO₂. *Glob. Chang. Biol.* 7 (2), 127–145.
- Broge, N.H., Leblanc, E., 2000. Comparing prediction power and stability of broadband and hyperspectral vegetation indices for estimation of green leaf area index and canopy chlorophyll density. *Remote Sens. Environ.* 76, 156–172.
- Calderón, R., Navas-Cortés, J.A., Zarco-Tejada, P.J., 2015. Early detection and quantification of *Verticillium* wilt in olive using Hyperspectral and thermal imagery over large areas. *Remote Sens.* 7, 5584–5610. <https://doi.org/10.3390/rs70505584>.
- Camino, C., González-Dugo, V., Hernández, P., Zarco-Tejada, P.J., 2019. Radiative transfer Vcmax estimation from hyperspectral imagery and SIF retrievals to assess photosynthetic performance in rainfed and irrigated plant phenotyping trials. *Remote Sensing of Environment* 231, 111186.
- Cescatti, A., 1997. Modelling the radiative transfer in discontinuous canopies of asymmetric crowns. I. Model structure and algorithms. *Ecol. Model.* 101, 263–274.
- Chaerle, L., Hagenbeek, D., Vanrobaeys, X., Van der Straeten, D., 2007. Early detection of nutrient and biotic stress in *Phaseolus vulgaris*. *Int. J. Remote Sens.* 28 (16), 3479–3492.
- Cheng, T., Rivard, B., Sanchez-Azofeifa, A., 2011. Spectroscopic determination of leaf water content using continuous wavelet analysis. *Remote Sens. Environ.* 115, 659–670.
- Collatz, G.J., Ball, J.T., Grivet, C., Berry, J.A., 1991. Physiological and environmental regulation of stomatal conductance, photosynthesis and transpiration: a model that includes a laminar boundary layer. *Agric. For. Meteorol.* 54, 107–136.
- Combal, B., Baret, F., Poilvé, H., Polverin, U., 2001. Using multispectral reflectance to retrieve LAI and chlorophyll content of maize and soybean. In: Leroy, M. (Ed.), *Physical measurements and signatures in remote sensing*, Aussois, France, pp. 499–504.
- Combal, B., Baret, F., Weiss, M., Trubuil, A., Macé, D., Pragnère, A., Myneni, R., Knyazikhin, Y., Wang, L., 2003. Retrieval of canopy biophysical variables from bidirectional reflectance: using prior information to solve the ill-posed inverse problem. *Remote Sens. Environ.* 84 (1), 1–15.
- Courault, D., Seguin, B., Olioso, A., 2005. Review on estimation of evapotranspiration from remote sensing data: from empirical to numerical modeling approaches. *Irrig. Drain. Syst.* 19, 223–249.
- Cowan, I.R., 1978. In: Preston, R.D., Woolhouse, H.W.B.T.-A. (Eds.), *Stomatal Behaviour and Environment*. Academic Press, pp. 117–228. [https://doi.org/10.1016/S0065-2296\(08\)60370-5](https://doi.org/10.1016/S0065-2296(08)60370-5).
- Damm, A., Erler, A., Hillen, W., Meroni, M., Schaepman, M.E., Verhoef, W., Rascher, U., 2011. Modeling the impact of spectral sensor configurations on the FLD retrieval accuracy of sun-induced chlorophyll fluorescence. *Remote Sens. Environ.* 115, 1882–1892.
- Damm, A., Guanter, L., Laurent, V.C.E., Schaepman, M.E., Schickling, A., Rascher, U., 2014. FLD-based retrieval of sun-induced chlorophyll fluorescence from medium spectral resolution airborne spectroscopy data. *Remote Sens. Environ.* 147, 256–266.
- Damm, A., Guanter, L., Paul-Limoges, E., van der Tol, C., Hueni, A., Buchmann, N., Eugster, W., Ammann, C., Schaepman, M.E., 2015a. Far-red sun-induced chlorophyll fluorescence shows ecosystem-specific relationships to gross primary production: an assessment based on observational and approaches. *Remote Sens. Environ.* 166, 91–105.
- Damm, A., Guanter, L., Verhoef, W., Schaepfer, D., Garbari, S., Schaepman, M.E., 2015b. Impact of varying irradiance on vegetation indices and chlorophyll fluorescence derived from spectroscopy data. *Remote Sens. Environ.* 156, 202–215.
- Demmig, B., Winter, K., Krüger, A., Czygan, F.C., 1987. Photoinhibition and zeaxanthin formation in intact leaves: a possible role of the xanthophyll cycle in the dissipation of excess light energy. *Plant Physiol.* 84, 218–224.
- Demmig-Adams, B., 1990. Carotenoids and photoprotection in plants: a role for the xanthophyll zeaxanthin. *Biochimica et Biophysica Acta (BBA) – Bioenergetics* 1020 (1), 1–24.
- Dungan, R.J., Turnbull, M.H., Kelly, D., 2007. The carbon costs for host trees of a phloem-feeding herbivore. *J. Ecol.* 95, 603–613.
- Egea, G., Gonzalez-Real, M.M., Baille, A., Nortés, P.A., Diaz-Espejo, A., 2011. Disentangling the contributions of ontogeny and water stress to photosynthetic limitations in almond trees. *Plant, Cell and Environment* 34, 962–979.
- Egea, G., Gonzalez-Real, M.M., Baille, A., Nortés, P.A., Conesa, M.R., Ruiz-Salleres, I., 2012. Effects of water stress on irradiance acclimation of leaf traits in almond trees. *Tree Physiol.* 32, 450–463.
- Espadafor, M., Orgaz, F., Testi, L., Lorite, I.J., Gonzalez-Dugo, V., Fereres, E., 2017. Responses of transpiration and transpiration efficiency of almond trees to moderate stress deficits. *Sci. Hortic.* 225, 6–14.
- Evain, S., Flexas, J., Moya, I., 2004. A new instrument for passive remote sensing: 2. Measurement of leaf and canopy reflectance changes at 531 nm and their relationship with photosynthesis and chlorophyll fluorescence. *Remote Sens. Environ.* 91, 175–185.
- Farquhar, G.D., von Caemmerer, S., Berry, J.A., 1980. A biochemical-model of photosynthetic CO₂ assimilation in leaves of C-3 species. *Planta* 149, 78–90.
- Fereres, E., Goldhamer, D., Sadras, V., 2012. Yield response to water of fruit trees and vines: guidelines. In: Steduto, P., Hsiao, T.C., Fereres, E., Raes, D. (Eds.), *CRop yield response to water*. Irrigation and drainage paper. Food and agriculture Organization of the United Nations (FAO), Rome, pp. 246–296.
- Filella, I., Amaro, T., Araus, J.L., Peñuelas, J., 1996. Relationship between photosynthetic radiation use efficiency of barley canopies and the photochemical reflectance index (PRI). *Physiol. Plant.* 96, 211–216.
- Flexas, J., Briantais, J.M., Cerovic, Z., Medrano, H., Moya, I., 2000. Steady-state and maximum chlorophyll fluorescence responses to water stress in grapevine leaves: a new remote sensing system. *Remote Sens. Environ.* 73, 282–297.
- Flexas, J., Escalona, J.M., Evain, S., Gulias, J., Moya, I., Osmond, C.B., et al., 2002. Steady-state chlorophyll fluorescence (Fs) measurements as a tool to follow variations of net CO₂ assimilation and stomatal conductance during water-stress in C-3 plants. *Physiol. Plant.* 114 (2), 231–240.
- Frankenberg, C., Fisher, J.B., Worden, J., Badgley, G., Saatchi, S.S., Lee, J.E., Toon, G.C., Butz, A., Jung, M., Kuze, A., Yokota, T., 2011. New global observations of the terrestrial carbon cycle from GOSAT: patterns of plant fluorescence with gross primary productivity. *Geophys. Res. Lett.* 38 <https://doi.org/10.1029/2011GL048738>.
- Gamon, J., Peñuelas, J.A., Field, C.B., 1992. A narrow-waveband spectral index that tracks diurnal changes in photosynthetic efficiency. *Remote Sens. Environ.* 41, 35–44.
- Gamon, J.A., Filella, I., Peñuelas, J., 1993. The dynamic 531 nm reflectance signal: A survey of twenty angiosperm species. In: Yamamoto, H.Y., Smith, C.M. (Eds.), 1993. *Photosynthetic Responses to the Environment*. American Society of Plant Physiologists, Rockville, MD, pp. 172–177.
- Gamon, J.A., Serrano, L., Surfus, J.S., 1997. The photochemical reflectance index: an optical indicator of photosynthetic radiation use efficiency across species, functional types, and nutrient levels. *Oecologia* 112 (4), 492–501.
- Guan, K., Berry, J.A., Zhang, Y., Joiner, J., Guanter, L., Bagley, G., Lobell, D.B., 2016. Improving the monitoring of crop productivity using spaceborne solar-induced fluorescence. *Global Change Biol.* 22, 716–726. <https://doi.org/10.1111/gcb.13136>.
- Guanter, L., Zhang, Y., Jung, M., Joiner, J., Voigt, M., Berry, J.A., Griffis, T.J., 2014. Global and time-resolved monitoring of crop photosynthesis with chlorophyll fluorescence. *Proceedings of the National Academy of Sciences (PNAS)*. <https://doi.org/10.1073/pnas.132008111>.
- Gueymard, C., 1995. SMARTS, a simple model of the atmospheric Radiative transfer of sunshine: algorithms and performance assessment. In: Florida solar energy center, cocoa, FL technical report no. FSEC-PF-270-95.
- Gueymard, C.A., Myers, D., Emery, K., 2002. Proposed reference irradiance spectra for solar energy systems testing. *Sol. Energy* 73, 443–467. [https://doi.org/10.1016/S0038-092X\(03\)00005-7](https://doi.org/10.1016/S0038-092X(03)00005-7).
- Haboudane, D., Miller, J.R., Tremblay, N., Zarco-Tejada, P.J., Dextraze, L., 2002. Integrated narrow-band vegetation indices for prediction of crop chlorophyll content for application to precision agriculture. *Remote Sens. Environ.* 81, 416–426.
- Haboudane, D., Miller, J.R., Pattey, E., Zarco-Tejada, P.J., Strachan, I.B., 2004. Hyperspectral vegetation indices and novel algorithms for predicting green LAI of crop canopies: modeling and validation in the context of precision agriculture. *Remote Sens. Environ.* 90, 337–352.
- Hernández-Clemente, R., Hornero, A., Mottus, M., Penuelas, J., González-Dugo, V., Jiménez, J.C., Suárez, L., Alonso, L., Zarco-Tejada, P.J., 2019. Early diagnosis of vegetation health from high-resolution Hyperspectral and thermal imagery: lessons learned from empirical relationships and Radiative transfer Modelling. *Current Forestry Reports* 5, 169–183. <https://doi.org/10.1007/s40725-019-00096-1>.
- Hsiao, T.C., Bradford, K.J., 1983. Physiological consequences of cellular water deficits. In: Taylor, H.M., Wayne, J.R., Thomas, S.R. (Eds.), *Limitations to Efficient Water Use in Crop Production*. ASA, CSSA, SSSA, Madison, WI, pp. 227–265. <https://doi.org/10.2134/1983.limitationstoefficientwateruse.c15>.

- Hsiao, T.C., Fereres, E., Acevedo, E., Henderson, D.W., 1976. Water stress and dynamics of growth and yield of crop plants. In: Lange, O.L., Kappen, L., Schulze, E.D. (Eds.), *Water and plant life, Ecological studies (analysis and synthesis)*, vol 19. Springer, Berlin, Heidelberg.
- Huete, A., Didan, K., Miura, T., Rodriguez, E.P., Gao, X., Ferreira, L.G., 2002. Overview of the radiometric and biophysical performance of the MODIS vegetation indices. *Remote Sens. Environ.* 83, 195–213.
- Ihuoma, S.O., Madramootoo, C.A., 2017. Recent advances in crop water stress detection. *Computer and Electronics in Agriculture* 141, 267–275.
- Jacquemoud, S., Verhoef, W., Baret, W., Bacour, C., Zarco-Tejada, P.J., Asner, G.P., François, C., Ustin, S.L., 2009. PROSPECT+SAIL models: a review of use for vegetation characterization. *Remote Sens. Environ.* 113, S56–S66.
- Kattenborn, T., Fassnacht, F.E., Pierce, S., Lopatin, J., Grim, J.P., Schmidlein, S., 2017. Linking plant strategies and plant traits derived by radiative transfer modelling. *J. Veg. Sci.* 28, 717–727.
- Kimball, B.A., 1983. Carbon dioxide and agricultural yield: an assemblage and analysis of 430 prior observations. *Agron. J.* 75, 779–788.
- Knohl, A., Buchmann, N., 2005. Partitioning the net CO₂ flux of a deciduous forest into respiration and assimilation using stable carbon isotopes. *Glob. Biogeochem. Cycles* 19 (4). <https://doi.org/10.1029/2004GB002301>.
- Koffi, E.N., Rayner, P.J., Norton, A.J., Frankenberg, C., Scholze, M., 2015. Investigating the usefulness of satellite-derived fluorescence data in inferring gross primary productivity within the carbon cycle data assimilation system. *Biogeosciences* 12, 4067–4084.
- Krause, G.H., Weis, E., 1991. Chlorophyll fluorescence and photosynthesis: the basics. *Annu. Rev. Plant Physiol. Plant Mol. Biol.* 42, 313–349.
- Laurent, V.C.E., Schaepment, M.E., Verhoef, W., Weyeremann, J., Chavez, R.O., 2014. Bayesian object-based estimation of LAI and chlorophyll from a simulated Sentinel-2 top-of-atmosphere radiance image. *Remote Sens. Environ.* 140, 318–329.
- Law, B.E., Cescatti, A., Baldocchi, D.D., 2001. Leaf area distribution and radiative transfer in open-canopy forests: implications for mass and energy exchange. *Tree Physiol.* 21 (12–13), 777–787.
- Lichtenthaler, H.K., Wenzel, O., Buschmann, C., Gitelson, A., 1998. Plant stress detection by reflectance and fluorescence. *Ann. N. Y. Acad. Sci.* 851, 271–285.
- Lobell, D.B., Cassman, K.G., Field, C.B., 2009. Crop yield gaps: their importance, magnitudes, and causes. *Annu. Rev. Environ. Resour.* 34, 179–204.
- Long, S.P., Marshall-Colon, A., Zhu, X.G., 2015. Meeting the global food demand of the future by engineering crop photosynthesis and yield potential. *Cell* 161 (1), 56–66.
- Lopez-Lopez, M., Espadafor, M., Testi, L., Lorite, L.J., Orgaz, F., Fereres, E., 2018. Water use efficiency of irrigated almond trees when subjected to water deficits. *Agric. Water Manag.* 195, 84–93.
- Lucieer, A., Malenovskiy, Z., Veness, T., Wallace, L., 2014. HyperUAS - imaging spectroscopy from a multirotor unmanned aircraft system. *Journal of Field Robotics* 31 (4), 571–590.
- Meroni, M., Rossini, M., Guanter, L., Alonso, L., Rascher, U., Colombo, R., 2009. Remote sensing of solar-induced chlorophyll fluorescence: review of methods and applications. *Remote Sens. Environ.* 113, 2037–2051.
- Mittermayr, C.R., Tan, H.W., Brown, S.D., 2001. Robust calibration with respect to background variation. *Appl. Spectrosc.* 55, 827–833.
- Mohammed, G.H., Binder, W.D., Gillies, S.L., 1995. Chlorophyll fluorescence: a review of its practical forestry applications and instrumentation. *Scand. J. For. Res.* 10, 383–410.
- Mohammed, G.H., Colombo, R., Middleton, E.M., Rascher, U., van der Tol, C., Nedbal, L., Goulas, Y., Pérez-Priego, O., Damm, A., Meroni, M., Joiner, J., Cogliati, S., Verhoef, W., Malenovskiy, Z., Gastellu-Etchegorry, J.P., Miller, J.R., Guanter, L., Moreno, J., Moya, I., Berry, J.A., Frankenberg, C., Zarco-Tejada, P.J., 2019. Remote sensing of solar-induced chlorophyll fluorescence (SIF) in vegetation: 50 years of progress. *Remote Sens. Environ.* 231, 111177. <https://doi.org/10.1016/j.rse.2019.04.030>.
- Moya, I., Camenen, L., Evain, S., Goulas, Y., Cerovic, Z.G., Latouche, G., Flexas, J., Ounis, A., 2004. A new instrument for passive remote sensing: 1. Measurements of sunlight-induced chlorophyll fluorescence. *Remote Sens. Environ.* 91, 186–197.
- Nichol, C.J., Lloyd, J., Shibtsova, O., Arneith, A., Röser, C., Knohl, A., Matsubara, S., Grace, J., 2002. Remote sensing of photosynthetic-light-use-efficiency of a Siberian boreal forest. *Tellus* 54B, 677–687.
- Papageorgiou, G., 1975. Chlorophyll fluorescence: An intrinsic probe of photosynthesis. In: Govindjee (Ed.), *Bioenergetics of Photosynthesis*. Academic Press, New York, pp. 319–371.
- Peñuelas, J., Gamon, J.A., Fredeen, A.L., Merino, J., Field, C.B., 1994. Reflectance indices associated with physiological changes in nitrogen- and water-limited sunflower leaves. *Remote Sens. Environ.* 48, 135–146.
- Peñuelas, J., Filella, I., Baret, F., 1995. Semiempirical indices to assess carotenoids/chlorophyll a ratio from leaf spectral reflectance. *Photosynthetica* 31, 221–230.
- Pérez-Priego, O., Zarco-Tejada, P.J., Miller, J.R., Sepulcre-Cantó, G., Fereres, E., 2005. Detection of water stress in orchard trees with a high-resolution spectrometer through chlorophyll fluorescence in-filling of the O₂-a band. *IEEE Trans. Geosci. Remote Sens.* 43, 2860–2868.
- Plascyk, J.A., Gabriel, F.C., 1975. The Fraunhofer line discriminator MKII an airborne instrument for precise and standardized ecological luminescence measurement. *IEEE Trans. Instrum. Meas.* 24, 306–313.
- Raggi, V., 1995. CO₂ assimilation, respiration and chlorophyll fluorescence in peach leaves infected by *Taphrina deformans*. *Physiol. Plant.* 93, 540–544.
- Rascher, U., Agati, G., Alonso, L., Cecchi, G., Champagne, S., Colombo, R., et al., 2009. CEFLES2: the remote sensing component to quantify photosynthetic efficiency from the leaf to the region by measuring sun-induced fluorescence in the oxygen absorption bands. *Biogeosci. Discuss.* 6 (7), 2217–2266.
- Reichstein, M., Falge, E., Baldocchi, D., Papale, D., Aubinet, M., Berbigier, P., Bernhofer, C., Buchmann, N., et al., 2005. On the separation of net ecosystem exchange into assimilation and ecosystem respiration: review and improved algorithm. *Glob. Chang. Biol.* 11, 1424–1439.
- Rosema, A., Verhoef, W., Noorbergen, H., Borgesius, J.J., 1992. A new forest light interaction model in support of forest monitoring. *Remote Sens. Environ.* 42 (1), 23–41.
- Rougean, J.L., Breon, F.M., 1995. Estimating PAR absorbed by vegetation from bidirectional reflectance measurements. *Remote Sens. Environ.* 51, 375–384.
- Rouse, J.W., Hass, R.H., Schell, J.A., Deering, D.W., 1973. Monitoring vegetation systems 742 in the great plains with ERTS. *Third earth Resour. Technol. Satell. Symp.* 1, 309–317. 743 doi:citeulike-article-id:12009708.
- Running, S.W., Baldocchi, D.D., Turner, D.P., Gower, S.T., Bakwin, P.S., Hibbard, K.A., 1999. A global terrestrial monitoring network integrating tower fluxes, flask sampling, ecosystem modeling and EOS satellite data. *Remote Sens. Environ.* 70 (1), 108–127.
- Savitzky, G., Golay, M.J.E., 1964. Smoothing and differentiation of data by simplified least squares procedures. *Anal. Chem.* 36 (8), 1627–1639. <https://doi.org/10.1021/ac60214a047>.
- Schurr, U., Walter, A., Rascher, U., 2006. Functional dynamics of plant growth and photosynthesis – from steady-state to dynamics – from homogeneity to heterogeneity. *Plant, Cell and Environment* 29, 340–352.
- Serbin, S.P., Dillaway, D.N., Kruger, E.L., Townsend, P.A., 2012. Leaf optical properties reflect variation in photosynthetic metabolism and its sensitivity to temperature. *J. Exp. Bot.* 63, 489–502. <https://doi.org/10.1093/jxb/err294>.
- Serbin, S.P., Singh, A., Desai, A.R., Dubois, S.G., Jablonski, A.D., Kingdon, C.C., Kruger, E.L., Townsend, P.A. (2015). Remotely estimating photosynthetic capacity, and its response to temperature, in vegetation canopies using imaging spectroscopy. *Remote Sens. Environ.*, 167, 78–87.
- Stagakis, S., González-Dugo, V., Cid, P., Guillén-Climent, M.L., Zarco-Tejada, P.J., 2012. Monitoring water stress and fruit quality in an orange orchard under regulated deficit irrigation using narrow-band structural and physiological remote sensing indices. *ISPRS J. Photogramm. Remote Sens.* 71, 47–61.
- Styllinski, C.D., Oechel, W.C., Gamon, J.A., Tissue, D.T., Miglietta, F., Raschi, A., 2000. Effects of lifelong [CO₂] enrichment on carboxylation and light utilization of *Quercus pubescens* Willd. Examined with gas exchange, biochemistry and optical techniques. *Plant, Cell and Environment* 23, 1353–1362.
- Suárez, L., Zarco-Tejada, P.J., Sepulcre-Cantó, G., Pérez-Priego, O., Miller, J.R., Jiménez-Muñoz, J.C., Sobrino, J., 2008. Assessing canopy PRI for water stress detection with diurnal airborne imagery. *Remote Sens. Environ.* 112, 560–575.
- Suárez, L., Zarco-Tejada, P.J., Berni, J.A.J., González-Dugo, V., Fereres, E., 2009. Modelling PRI for water stress detection using Radiative transfer models. *Remote Sens. Environ.* 113, 730–744.
- Suárez, L., Zarco-Tejada, P.J., González-Dugo, V., Berni, J.A.J., Sagardoy, R., Morales, F., Fereres, E., 2010. Detecting water stress effects on fruit quality in orchards with time-series PRI airborne imagery. *Remote Sens. Environ.* 114, 286–298.
- Thenot, F., Méthy, M., Winkel, T., 2002. The photochemical reflectance index (PRI) as a water-stress index. *Int. J. Remote Sens.* 23 (23), 5135–5139.
- Tremblay, N., Wang, Z., Cerovic, Z.G., 2011. Sensing crop nitrogen status with fluorescence indicators A review. *Agronomy for sustainable Development* 32, 451–464.
- Trotter, G.M., Whitehead, D., Pinkney, E.J., 2002. The photochemical reflectance index as a measure of photosynthetic light use efficiency for plants with varying foliar nitrogen contents. *Int. J. Remote Sens.* 23 (6), 1207–1212.
- Van der Tol, C., Verhoef, W., Timmermans, J., Verhoef, A., Su, Z., 2009. An integrated model of soil-canopy spectral radiances, photosynthesis, fluorescence, temperature and energy balance. *Biogeosciences* 6 (12), 3109–3129.
- Van der Tol, C., Berry, J.A., Campbell, P.K.E., Rascher, U., 2014. Models of fluorescence and photosynthesis for interpreting measurements of solar-induced chlorophyll fluorescence. *J. Geophys. Res. Biogeosci.* 119 (12), 2312–2327.
- Verhoef, W., 1984. Light scattering by leaf layers with application to canopy reflectance modeling: the SAIL model. *Remote Sens. Environ.* 16, 125–141.
- Verma, M., Schimel, D., Evans, B., Frankenberg, C., Beringer, J., Drewry, D.T., Magney, T., Marang, I., Hutley, L., Moore, C., Eldering, A., 2017. Effect of environmental conditions on the relationship between solar-induced fluorescence and gross primary productivity at an OzFlux grassland site. *J. Geophys. Res. Biogeosci.* 122, 716–733. <https://doi.org/10.1002/2016JG003580>.
- Verrelst, J., Schaepman, M.E., Malenovskiy, Z., Clevers, J.G.P.W., 2010. Effects of woody elements on simulated canopy reflectance: implications for forest chlorophyll content retrieval. *Remote Sens. Environ.* 114 (3), 647–656.
- Verstraete, M.M., Pinty, B., Dickinson, R.E., 1990. A physical model of the bidirectional reflectance of vegetation canopies. 1. Theory. *J. Geophys. Res.* 95, 11765–11775.
- Vilfan, N., van der Tol, C., Muller, O., Rascher, U., Verhoef, W., 2016. Fluspect-B: a model for leaf fluorescence, reflectance and transmittance spectra. *Remote Sens. Environ.* 186, 596–615.
- Widlowski, J.-L., Pinty, B., Lavergne, T., Verstraete, M.M., Gobron, N. (2006) Horizontal radiation transport in 3-D forest canopies at multiple spatial resolutions: simulated impact on canopy absorption. *Remote Sens. Environ.*, 103, 379–397.
- Woodgate, W., Suarez, L., van Gorsel, E., Cernusak, L., Devilla, R., Held, A., Hughes, D., Norton, A., 2019. Tri-PRI: a three band reflectance index tracking dynamic photoprotective mechanisms in a mature eucalypt forest. *Agriculture and Forest Meteorology* 272–273, 187–201.
- Woodward, F.I., Smith, T.M., Emanuel, W.R., 1995. A global land primary productivity and phytogeography model. *Glob. Biogeochem. Cycles* 9, 471–490.

- Xu, L., Baldocchi, D.D., 2003. Seasonal trends in photosynthetic parameters and stomatal conductance of blue oak (*Quercus douglasii*) under prolonged summer drought and high temperature. *Tree Physiol.* 23, 865–877.
- Yang, P., Verhoef, W., van der Tol, C., 2017. The mSCOPE model: a simple adaptation to the SCOPE model to describe reflectance, fluorescence and photosynthesis of vertically heterogeneous canopies. *Remote Sens. Environ.* 201, 1–11.
- Zarco-Tejada, P.J., Miller, J.R., Mohammed, G.H., Noland, T.L., Sampson, P.H., 2001. Scaling-up and model inversion methods with narrow-band optical indices for chlorophyll content estimation in closed Forest canopies with Hyperspectral data. *IEEE Trans. Geosci. Remote Sens.* 39 (7), 1491–1507.
- Zarco-Tejada, P.J., Berni, J.A.J., Suárez, L., Sepulcre-Cantó, G., Morales, F., Miller, J.R., 2009. Imaging chlorophyll fluorescence from an airborne narrow-band multispectral camera for vegetation stress detection. *Remote Sens. Environ.* 113, 1262–1275.
- Zarco-Tejada, P.J., González-Dugo, V., Berni, J.A.J., 2012. Fluorescence, temperature and narrow-band indices acquired from a UAV platform for water stress detection using a micro-hyperspectral imager and a thermal camera. *Remote Sens. Environ.* 117, 322–337.
- Zarco-Tejada, P.J., Suárez, L., González-Dugo, V., 2013a. Spatial resolution effects on chlorophyll fluorescence retrievals in a heterogeneous canopy using hyperspectral imagery and radiative transfer simulation. *Geoscience and Remote Sensing Letters*. <https://doi.org/10.1109/LGRS.2013.2252877>.
- Zarco-Tejada, P.J., González-Dugo, V., Williams, L.E., Suárez, L., Berni, J.A.J., Goldammer, D., Fereres, E., 2013b. A PRI-based water stress index combining structural and chlorophyll effects: assessment using diurnal narrow-band airborne imagery and the CWSI thermal index. *Remote Sens. Environ.* 138, 38–50.
- Zarco-Tejada, P.J., González-Dugo, M.V., Fereres, F., 2016. Seasonal stability of chlorophyll fluorescence quantified from airborne hyperspectral imagery as an indicator of net photosynthesis in the context of precision agriculture. *Remote Sens. Environ.* 179 (15), 89–103.
- Zarco-Tejada, P.J., Camino, C., Beck, P.S.A., Calderon, R., Hornero, A., Hernández-Clemente, R., Kattenborn, T., Montes-Borrego, M., Susca, L., Morelli, M., Gonzalez-Dugo, V., North, P.R.J., Landa, B.B., Boscia, D., Saponari, M., Navas-Cortes, J.A., 2018. Pre-visual symptoms of *Xylella fastidiosa* infection revealed in spectral plant-trait alterations. *Nature Plants*. <https://doi.org/10.1038/s41477-018-0189-7>.
- Zhang, Y., Guanter, L., Berry, J.A., Joiner, J., van der Tol, C., Huete, A., Gitelson, A., Voigt, M., Köhler, P., 2014. Estimation of vegetation photosynthetic capacity from space-based measurements of chlorophyll fluorescence for terrestrial biosphere models. *Glob. Chang. Biol.* 20, 3727–3742.
- Zhang, Y., Guanter, L., Joiner, J., Song, L., Guan, K., 2018. Spatially-explicit monitoring of crop photosynthetic capacity through the use of space-based chlorophyll fluorescence data. *Remote Sens. Environ.* 210, 362–374.